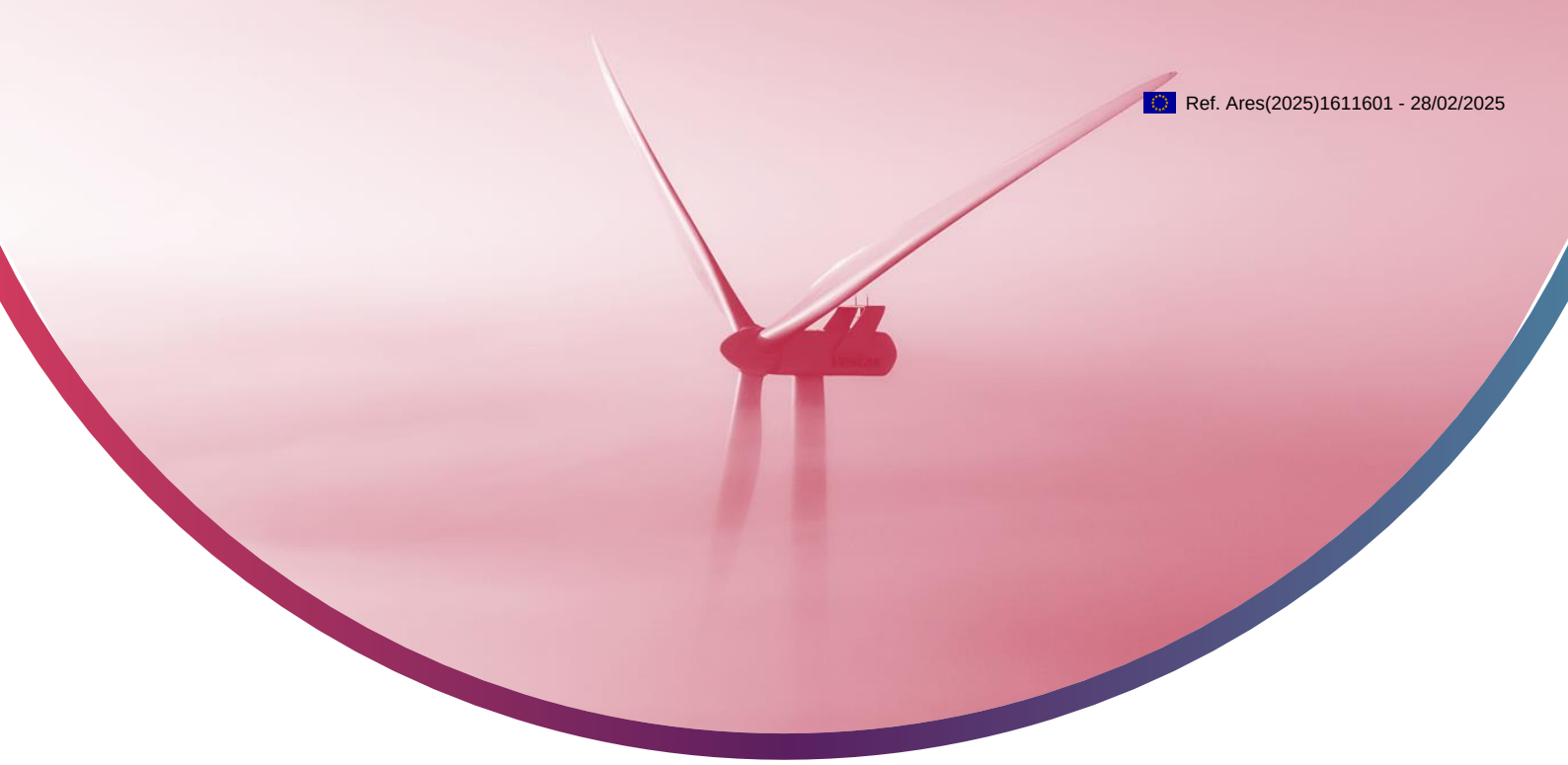

AiRE

D3.4 Numerical characterization of precipitation impingement on a rotating

Advanced study of the atmospheric flow Integrating REal climate conditions to enhance wind farm and wind turbine power production and increase components durability

Fraunhofer IWES

DOCUMENT INFORMATION

PROJECT INFORMATION	
GRANT AGREEMENT NUMBER	101083716
PROJECT TITLE	Advanced study of the atmospheric flow Integrating REal climate conditions to enhance wind farm and wind turbine power production and increase components durability
PROJECT ACRONYM	AIRE
FUNDING SCHEME	HORIZON-RIA
PROJECT COORDINATOR	CENER
START DATE OF THE PROJECT	1 January 2023
DURATION	48 months
CALL IDENTIFIER	HORIZON-CL5-2021-D3-03
PROJECT WEBSITE	https://aire-project.eu/

DELIVERABLE INFORMATION	
DELIVERABLE N° & TITLE	D3.4 Numerical characterization of precipitation impingement on rotating wind turbine
WP NO. & TITLE	T3.4 Study and modelling of rain impingement on rotating wind turbine
WP LEADER	Fraunhofer IWES
DELIVERABLE CREATOR	Fraunhofer IWES
CONTRIBUTING PARTNERS	Fraunhofer IWES, SGRE
AUTHORS	Mohsen Javaherianrad, Leo Höning, Johannes Nicolaas Theron, Hassan Kassem
REVIEWERS	Teijo Arponen (VTT), Beatriz Méndez (CENER)
CONTRACTUAL DEADLINE	M20
DELIVERY DATE TO EC	M26
DISSEMINATION LEVEL	PU - Public

DOCUMENT LOG			
VERSION	DATE	AUTHOR	DESCRIPTION OF CHANGE
V1.1	14.02.2025	Fraunhofer IWES	Initial version
V1.2	26.02.2025	Teijo Arponen (VTT), Beatriz Méndez (CENER)	Review feedback
V2.1	27.02.2025	Fraunhofer IWES	Second version
V2.2	27.02.2025	Laia Mencia (INV)	Review feedback
V3.1	28.02.2025	Beatriz Méndez (CENER)	Final version approval

DISCLAIMER

"Funded by the European Union. Views and opinions expressed are however those of the author(s) only and do not necessarily reflect those of the European Union. Neither the European Union nor the granting authority can be held responsible for them."

Content

Figure Index

Table index

Acronym Glossary

GA: Grant Agreement	**SC**: Steering Committee
CA: Consortium Agreement	**EEAB**: External Expert Advisory Board
PC: Project Coordinator	**EC:** European Commission
GAS: General Assembly	**PMH:** Project Management Handbook

Consortium partners

	Partner	Country	Short name
1	Centro Nacional de Energías Renovables	Spain	CENER
2	Danmarks Tekniske Universitet	Denmark	DTU
3	Teknologian Tutkimuskeskus	Finland	VTT
4	Frauhofer Gesellschaft zur Forderung der Angewandten Forschung	Germany	IWES
5	Siemens Gamesa Renewable Energy	Denmark	SGRE
6	Green Capital Power	Spain	CAPITAL
7	ENGIE	France	ENGIE
8	Consorcio para el diseño, construcción, equipamiento y explotación de la plataforma oceánica de Canarias	Spain	PLOCAN
8.1	Universidad de Las Palmas de Gran Canaria	Spain	ULPGC
9	Cartago Ventures	Spain	INV
10	Offshore Renewable Energy Catapult	UK	OREC

1 List of symbols and abbreviations

Symbol	Description	Units
A_p	Particle cross section	m^2
C_D	Drag coefficient	-
d_p	Particle diameter	m
F	Impact force	N
f_d	Schiller-Neumann Correction Factor	-
f_h	Probability density function	-
I	Raindrop Size Distribution Slope Parameter	mm^{-1}
I_p	Sphere moment of inertia	$kg.m^2$
LWC	Liquid water content	$gr.m^{-3}$
m_p	Particle mass	kg
N_o	Rain parameter	$m^{-3}\ mm^{-1}$
ODE	Ordinary differential equations	-
Q	Volumetric flow rate	$m^3.s^{-1}$
R	Rainfall rate	$mm.h^{-1}$
Re	Reynolds number	-
Re_p	Particle Reynolds number	-
R_h	Rain intensity	$mm.h^{-1}$
T	Torque acting on a particle	$kg{\cdot}m^2.s^{-2}$
U_∞	Freestream velocity	$m.s^{-1}$
V	Impact velocity	$m.s^{-1}$
V_∞	Freestream velocity	$m.s^{-1}$
Vt	Terminal velocity	$m.s^{-1}$

Greek symbols

ρ_p	Particle density	$kg.m^{-3}$
ω_p	Angular velocity	$rad.s^{-1}$

2 Abstract

All the measurement campaigns and model developments in the AIRE project are done with the one main objective in mind, namely understanding the realistic atmospheric conditions around wind turbines, specifically including the presence of rain. These operating conditions impact the performance of each wind turbine which is reflected on the AEP of an entire wind farm; be it by its mere presence in modifying flow conditions, or by its physical effect in modifying / eroding wind turbine components. Therefore, it is not surprising that erosion is the centre focus of the AIRE project. In the task on hand (T3.4), the objective is to study the rain impingement on a full rotating wind turbine (without considering the tower), specifically the IEA 15MW. Such study gives new insights into the rain droplet distribution in terms of droplet diameter and impact velocity. These two properties of rain droplet trajectory are the key inputs for any erosion-damage model. Unlike many previous studies to 2D airfoils, a blade section or a single blade, in T3.4 a full rotor is modelled under different rain conditions while varying the rain intensity rate and the corresponding rain diameter distribution.

Achieving that challenging goal requires high fidelity CFD simulations. The model used here resolves the motion of the wind field and tracks the particles of rain. This multi-phase approach (Eulerian - Lagrangian) is indeed computationally expensive. Therefore, IWES had to build the model step-by-step to make sure the predicted results would satisfy the general target of the AIRE project. Hence, this task started with studying flow over a 2D blade section (airfoil), then moving to 3D single blade simulations. Finally studying 3D full-rotor (3-blade) simulations. These steps are necessary not only because they are the building blocks of the target simulation, but also because having these three types of simulations give some insight into the benefits of each level of computational fidelity. This understanding shall help in AIRE and the industry to choose the appropriate level of fidelity during the blade design process in WP6. Therefore, this report shows these three levels, then comparing and contrasting these simulations.

Additionally, an extra 3D rotor of NREL 5MW has been included in this work. Having such a case widens the scope of this task and covers two sizes of turbines which represent legacy and modern turbines. The results show very strong correlations between the precipitation input distribution and the local rain distribution across the blade. The 3D single blade and full rotor show a clear advantage in terms of impact distribution compared to the 2D airfoil cases. The findings overall agree with those of actual site observations in terms of the location of erosion along the leading edge of the blade. The task has achieved its goals with some delays due to the high computational cost of the CFD simulations. However, the extra time allowed for additional cases and advanced post-processing of the results. The results and findings support the design of airfoils in WP6. Also, it can be used as input for the damage model in WP3 and the AIRE toolbox in WP4.

3 Introduction

Leading edge erosion has become a major concern, especially in the offshore wind energy industry where the combination of high rainfall and large rotors with high tip speeds lead to blade damage and measurable reduction in annual energy production (AEP). Even in cases where the structural integrity of the blades is not compromised, aerodynamic performance is affected because of reduced airfoil efficiency (Cl/Cd ratio) and the early onset of transition. This causes a reduction in power production. The primary cause of this damage is the repeated high-speed impact of rain droplets, which transfers kinetic energy to the blade surface, causing material erosion and altering the blade profile[1].

A one-way dependence is typically assumed between the flow and particle dynamics when analysing the erosion patterns. This means that while the flow influences the particles' motion, the reverse effect is negligible [2]. Erosion patterns are then computed in this project based on the particle-cloud data, which closely replicate those observed in actual wind turbines. As turbine blades rotate at high tip speeds, such as 95 m/s at rated conditions for a 15 MW turbine, they become more susceptible to erosion damage even under moderate rain conditions. This issue not only reduces the aerodynamic efficiency and increases maintenance costs but also shortens the lifespan of the blades, making it crucial to understand and mitigate rain erosion for optimizing energy yield and ensuring the long-term reliability of wind turbines.

4 Methodology

Within this work package the impact of rain particles on wind turbine rotor blades is studied using computational fluid dynamics (CFD) with a Lagrangian particle tracking algorithm. These two systems need to be analysed in a coupled way as described below.

- Phase-Coupling Mechanisms:

Phase-coupling mechanisms strongly influence the behavior of the continuous and dispersed phase. In general, we have three ways of coupling, one-way, two-way and four-way coupling. In this project we used one-way coupling, where we just consider the effect of flow on the particles. Two-way coupling considers the effect of particle and flow together simultaneously and in four-way coupling simulations the effect of particle-particle collisions is also taken into account [2].

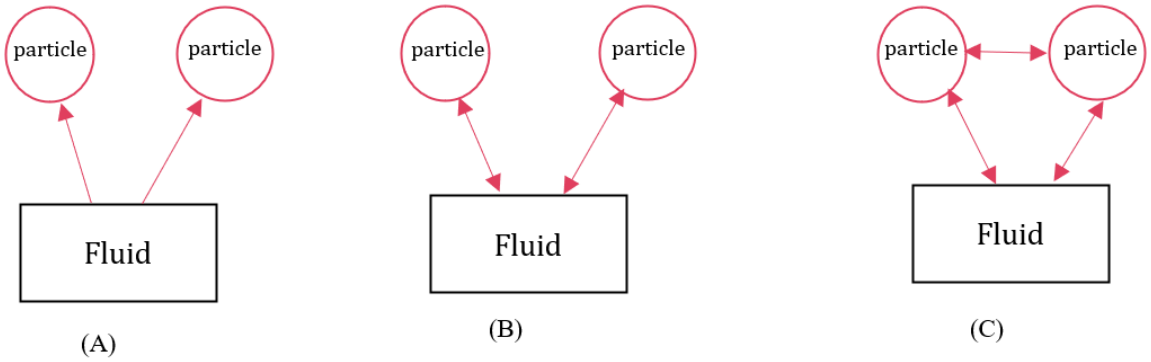

Figure 1. Fluid-particle coupling – A: one-way, B: two-way and C: four-way

4.1 Lagrangian particle tracking

The motion of particles within fluids is modelled using a Lagrangian approach, where a set of ordinary differential equations (ODEs) is solved along the particle's trajectory to determine changes in its position as well as the linear- and angular velocity components. This requires accounting for the various forces acting on the particle. For spherical particles, the ODEs used to calculate position and velocity are derived from Newton's second law of motion [2]:

$$\frac{dx_p}{dt} = u_p \quad (1)$$

$$m_p \frac{du_p}{dt} = \sum F_i \quad (2)$$

$$I_p \frac{d\omega_p}{dt} = T \quad (3)$$

Where $m_p = \frac{\rho_p d_p^3 \pi}{6}$ is the mass of particle and I_p is the moment of inertia for a sphere (defined by Equation 4):

$$I_p = 0.1 m_p d_p^2 \quad (4)$$

So F_i is the relevant forces acting on the particles, ω_p is the angular velocity and T being the torque acting on the rotating particle because of its interaction with fluid.

Analytical solutions for the various forces acting on particles are well-established for small Reynolds numbers (Stokes flow). To extend these solutions to higher Reynolds numbers, a coefficient C_D is

typically introduced in front of the force term. This coefficient is determined using empirical correlations obtained from experiments or direct numerical simulations. In most fluid-particle systems, the drag force plays a dominant role in influencing particle motion. For higher particle Reynolds numbers, the drag coefficient C_D is defined in Equation 5.

$$C_D = \frac{F_D}{\rho_D V^2 A_P} \quad 5$$

Where A_P is the cross-section of a particle.

The drag coefficient of a particle is dependent on the Reynolds number. The dependence of the drag coefficient of a spherical particle on Reynolds number is shown in Figure 2 taken from [3].

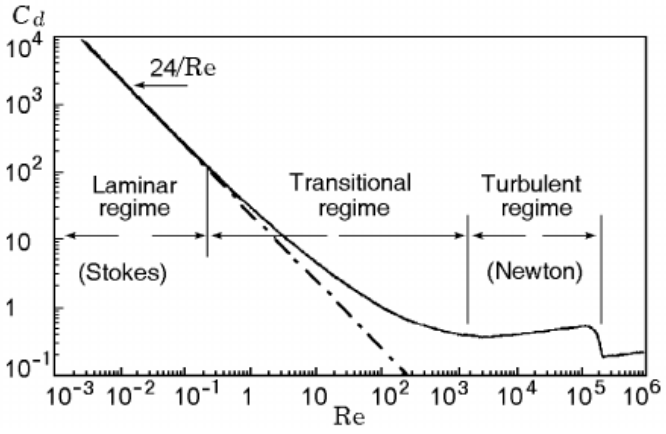

Figure 2. Drag coefficient as a function of the particle Reynolds number[4].

Viscous forces dominate at small Reynolds numbers. For this regime, Stokes proposed the analytic solution where $\boldsymbol{Re_P}$ is the particle Reynolds number defined in Equation 6 [3]:

$$C_D = \frac{24}{Re_P} \quad 6$$

For the transition region many correlations are proposed in literature, but the most frequent one is proposed by Schiller and Neumann (taken from [4]), which is valid up to $Re_P = 1000$.

$$C_D = \frac{24}{Re_P}\left(1 + 0.15{Re_P}^{0.687}\right) = \frac{24}{Re_P} f_d \quad 7$$

Above $Re_P = 1000$, the flow is fully turbulent, and the drag is constant until the critical Reynolds number is reached. This regime is known as Newton regime, with a constant drag coefficient:

$$C_D = 0.44 \quad 8$$

At the critical Reynold number ($2.5 \cdot 10^5$), the drag coefficient decreases due to transition from a laminar to a turbulent boundary layer around the particle.

Generally, the sub-critical model given by Clift and Gauvin [4] is used when Reynolds number is less than $2.5 \cdot 10^5$:

$$C_D = \frac{24}{Re_P}\left(1 + 0.15{Re_P}^{0.687}\right) + \frac{0.42}{1 + \frac{42500}{{Re_P}^{1.16}}} \quad 9$$

4.2 Characteristics of rain

4.2.1 Types of rain

There are different types of rain that are classified with N_0 (m^{-3} mm^{-1}) parameter and I (mm^{-1}). N_0 and I[1] dependent on the rain fall rate R (mm h^{-1}) [5].

Table 1. Values of N_0 and I for Different Types of Rainfall

Type of rainfall	N_0 (m^{-3} mm^{-1})	I (mm^{-1})
Drizzle	30,000	$I = 5.7 \times R^{-0.21}$
Widespread	7000	$I = 4.1 \times R^{-0.21}$
Thunderstorm	1400	$I = 3.0 \times R^{-0.21}$
Marshall and Palmer	8000	$I = 4.1 \times R^{-0.21}$

This classification was originally developed by Marshall and Palmer [6] who also suggested that I varied with the rainfall rate R. More recent studies showed that the values of N_0 and I are dependent on different types of rain, as shown in Table 1. Two important characteristic quantities generally used to describe the intensity of rain are the rainfall rate (R) and liquid water content (LWC). Rainfall rate is the linear accumulation depth at ground level per unit time (usually in unit of mm h^{-1}) used to characterize rainfall at ground level. Liquid water content is the mass of liquid water per unit volume, usually expressed in units of g m^{-3}.

4.2.2 Calculation of Liquid Water Content

In the wind tunnel environment, the LWC is calculated with the following relationship [7]:

$$LWC = \frac{KQ}{V_\infty HW} \tag{10}$$

where Q is the volumetric flow rate of water, V_∞ is the free-stream wind tunnel air velocity, H and W are the height and width of the water droplet spray region and K is the units conversion factor (K = 2225.8086).

In studying the effects of rain, the intensity is often described using either the rainfall rate (mm h^{-1}) or the liquid water content. Rainfall rates equal to or exceeding 100 mm h^{-1} are generally classified as heavy rain. For Marshall and Palmer-related rainfall, the relationship between LWC and R is given as [6]:

$$LWC = 0.0889R^{0.84} \tag{11}$$

4.2.3 Terminal velocity

Research on the terminal velocity of raindrops has a long history. The most widely used form of terminal velocity was developed by Markowitz [8] as a function of raindrop size and altitude. At low altitudes, it is given by:

$$V_t(d_p) = 9.58\left(1 - e^{-\left(\frac{d_p}{1.77}\right)^{1.147}}\right) \tag{12}$$

1 I is a parameter that determines the rate at which the number of raindrops decreases with increasing drop size

4.2.4 Droplet diameter distribution

To accurately represent the variability of rain, the rain flow intensity parameter R_h is used, which measures the amount of rainfall (in mm) that accumulates over one square meter in an hour. The relationship between rain flow intensity and droplet size can be described using a probability density function (f_h). This function accounts for the variability in droplet diameter dp for a given average R_h of the rain events at the site [9].

$$f_h(d_p, R_h) = 17.67 {d_p}^{0.67} \frac{2.25}{d_p} \left(\frac{d_p}{1.3 {R_h}^{0.232}} \right)^{2.25} \boldsymbol{exp}[-(\frac{\boldsymbol{d_p}}{\boldsymbol{1.3 {R_h}^{0.232}}})^{\boldsymbol{2.25}}] \quad 13$$

Figure 3 shows the droplet diameter probability density for different values of rain intensity calculated using Equation 13.

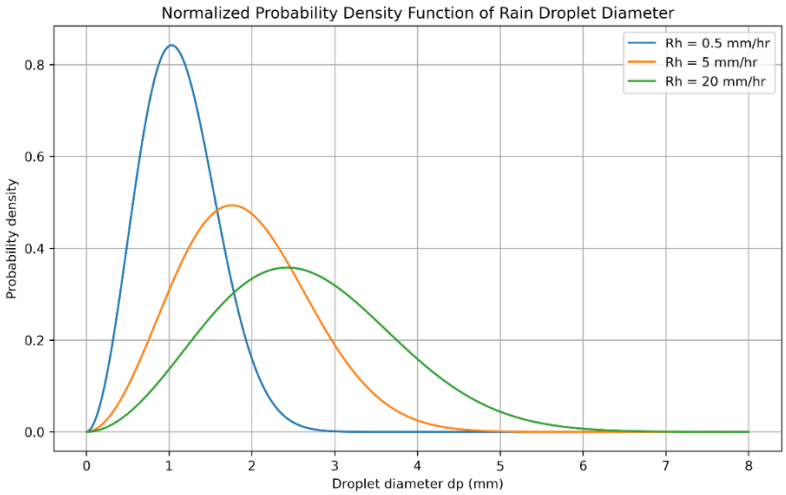

Figure 3. Theoretical PDF of droplet size distribution

4.2.5 Impact force

The impact force of each particle depends on the impact velocity V, the particle diameter d_p and the mass of the particle m_p in kg. This may be calculated with Equation 14 taken from [10].

$$F = \frac{m_p V^2}{d_p} \quad 14$$

5 Case studies

This study reports the results of three case studies, namely, a 2D airfoil case, a 3D blade case using a moving reference frame (MRF), and a full 3D rotor investigation. The full rotor simulation requires dynamic mesh movement, whereas the MRF technique adds a rotational velocity component to the stationary mesh. This allows to use steady state approach to solve rotational motion which reduces the computational time. Both the airfoil and the single blade MRF studies are based on the IEA 15 MW turbine. For the full rotor, the IEA 15MW [11] turbine as well as the NREL 5MW [12] turbine are investigated.

For the MRF case three different rain conditions are studied with rain intensities of 0.5, 5 and 20 mm/h, and for the full turbine case, 5 mm/h is used, which is near the common rain condition. An overview of all the cases that are discussed in this report, is given in Table 2. All simulations with 5 and 20 mm/h is discussed in the main body of this report; the case with 0.5mm/h is included in the Appendix (section 7).

Table 2. Overview of all simulated cases

Abbreviation	Simulation Type	WTG	R_h [mm/h]	Wind speed [m/s]	LWC	Section
2D15A5	2D airfoil	IEA 15MW	5	43.2[2]	0.34374	5.1
2D15A20	2D airfoil	IEA 15MW	20	43.2	1.10144	5.1
3D15MRF05C4	3D single blade	IEA 15MW	0.5	11.4	0.04969	7.1
3D15MRF5C4	3D single blade	IEA 15MW	5	11.4	0.34374	5.2.1
3D15MRF20C4	3D single blade	IEA 15MW	20	11.4	1.10144	5.2.1
3D15MRF5C0	3D single blade	IEA 15MW	5	10.0	0.34374	0
3D15MRF20C0	3D single blade	IEA 15MW	20	10.0	1.10144	0
3D5FR5	3D full rotor	NREL 5MW	5	11.4	0.34374	5.3.1
3D15FR5	3D full rotor	IEA 15MW	5	10.0	0.34374	5.3.2

5.1 2D blade section simulations 2D15A5 and 2D15A20

The first case is a 2D airfoil extracted from a mid-span section of the IEA 15MW blade. This is done to develop the necessary tools for pre- and post-processing of the rain particles, as well as to compare the capabilities of a computationally less-expensive 2D simulation in contrast to the full rotor configuration. Two rain intensities were considered for 2D simulations; 5mm/h and 20 mm/h. The corresponding flow conditions are given in Table 3.

Table 3 . Initial conditions

Free stream velocity	43.2 m/s
Angle of attack	6.462°
Chord length	3.5562 m
Simulated time	20 s

2 The 2D airfoil wind speed was calculated by taking into account the freestream velocity and the rotational velocity at its spanwise location on the IEA 15MW turbine.

Figure 4 shows the particle diameter distribution that impact the airfoil for the rain intensity rate of 5mm/h. The dashed line represents the theoretical particle diameter distribution that is used as the particle injection condition. It can be seen that the actual particle impact closely follows the injected size distribution, with some outliers for the particles binned at the size of 1mm and 1.5 mm.

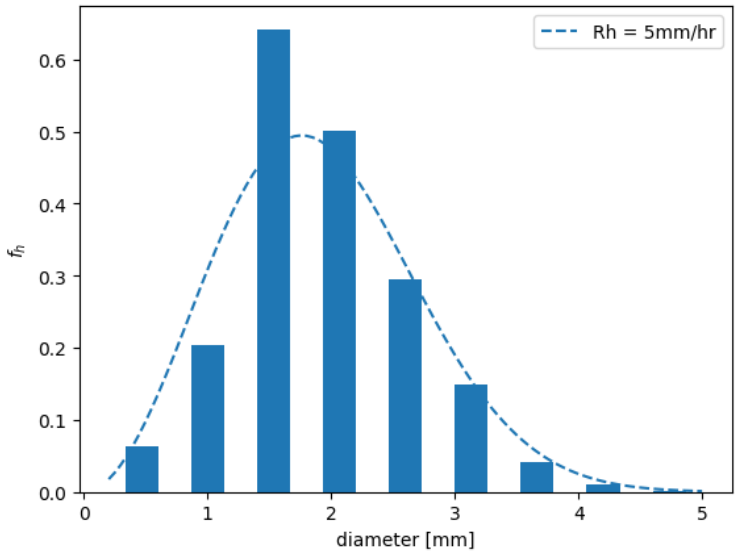

Figure 4. Particle diameter distribution for R_h=5mm/h that hit the airfoil (case 2D15A5)

Figure 5 depicts the impact force per unit area of the airfoil for the rain intensity rate of 5mm/h. A thin peak is observed at the leading edge (dashed line) of approximately 13kN/m^{2}s. This shows that under the given flow conditions, the area of highest impact is shifted towards the suction side. It has to be noted that within this study, the separation between pressure- and suction sides of the airfoils / blade sections is defined by the stagnation point and not by the leading edge of the blade. **In all impact-force plots in this report, the leading edge is denoted by dashed vertical lines.**

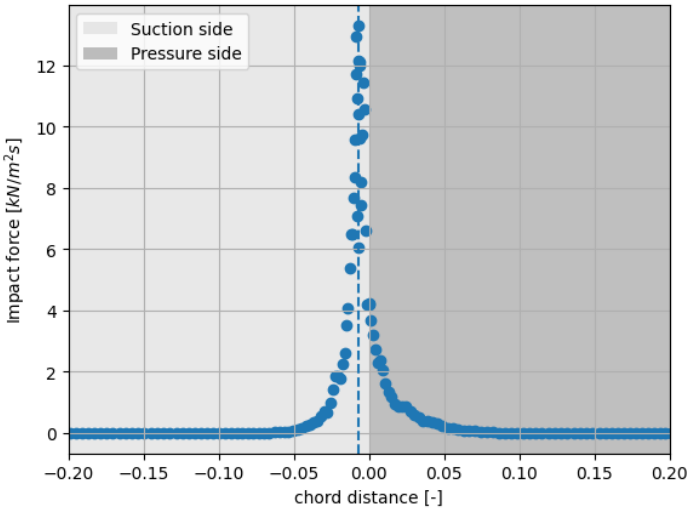

Figure 5. Impact force of the particles for the 2D airfoil for Rh=5mm/h (case 2D15A5)

Results for a rain intensity rate of 20 mm/h is presented in Figure 6. For this higher rainfall rate, the particle diameter distribution differs slightly to the 5mm/h rain intensity rate. Larger particle diameters are injected into the domain, which changes the resulting particle impact. The particle hit distribution (blue bars) roughly follows the theoretical input. Still an outlier can be seen for the particle diameter bin around 2mm.

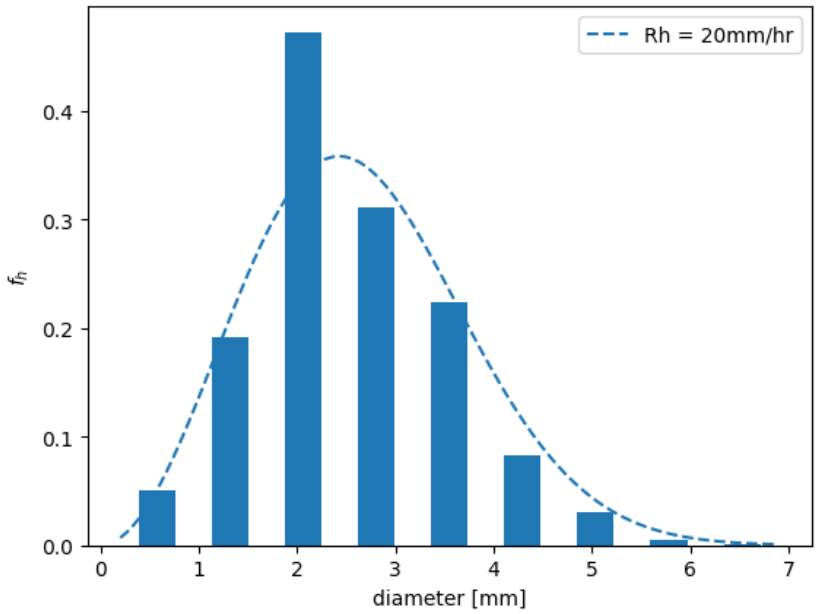

Figure 6. Particle diameter distribution for Rh=20mm/h that impact the airfoil. (case 2D15A20)

The resulting impact force per unit area per second is shown in Figure 7. Again, the impact zone is concentrated around the leading edge of the airfoil with a general shift towards the suction side. A maximum force of $35 kN/m^2 s$ can be seen, which is the direct result of the higher rain intensity rate.

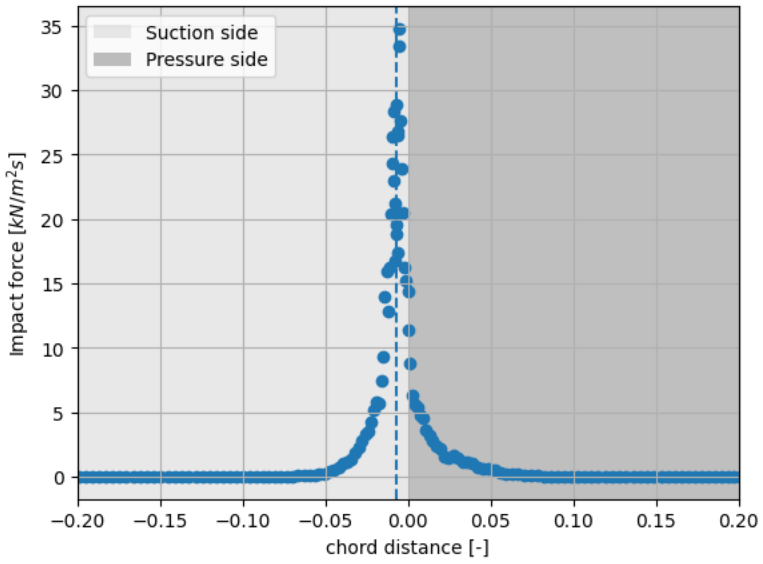

Figure 7. Impact force of the particles of the 2D airfoil for Rh=20mm/h (case 2D15A20).

5.2 Single blade (MRF cases) for the IEA 15MW blade

In the MRF method, a mesh zone is created around the rotating body, and during the simulation, the MRF zone rotates numerically while the body remains stationary. This allows the governing equations to be solved in a rotating reference frame, stabilizing the flow field with respect to the geometry. Within this study, the fluid simulation is performed first and then used as a "frozen" background field to the Lagrangian particle solver. Figure 8 illustrates the MRF simulation domain along with the corresponding patches (2D boundary surfaces).

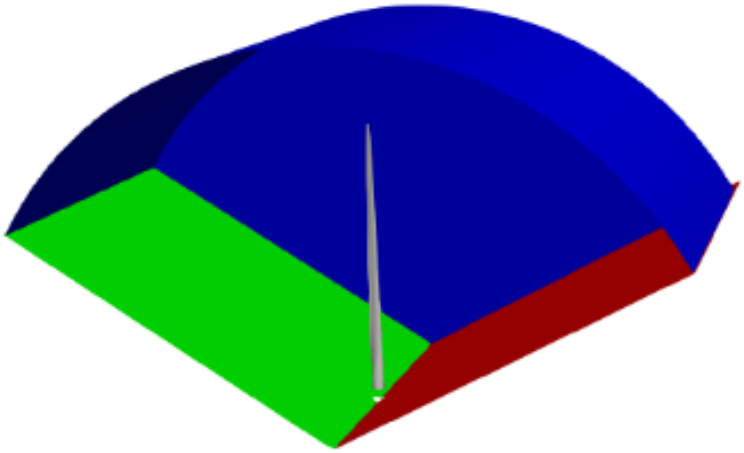

Figure 8. CFD domain used and definition of the boundary patches (red and green: left and right periodic; white: blade; blue: rotor disk)

The operating conditions used for the single blade MRF simulations are listed in Table 4.

Table 4. Initial conditions for the IEA 15MW MRF case with a cone angle=4°

Omega	0.56 rad/s
Inlet velocity	11.4 m/s
Blade length	117 m
Solid wall	No slip
Left and right	120° periodic rotation
Cone angle	4 degrees
Case name	3D15MRF5C4

To inject the particles into the pre-simulated background flow, 136 clouds are used, with each cloud having a fixed particle diameter distribution and a diameter of 6 meter. To initially accelerate the particles, their respective initial velocity is set to the local relative velocity between the incoming flow and the rotation speed of the blade section. The LWC is fixed for all the clouds along the blade by using Equation 15:

$$LWC = \frac{KQ}{V_\infty HW} \qquad 15$$

First, Equation 11 is used to calculate the LWC for different rain conditions. Then with help of Equation 15, the amount of particle in the domain is set to result in the same LWC. Table 5 summarizes the LWCs for the three investigated rain intensity rates.

Table 5. LWC for different rain intensity according to Marshall and Palmer

Rain intensity	0.5 mm/h	5 mm/h	20 mm/h
LWC	0.04969	0.34374	1.10144

Due to the LWC being a function of freestream velocity (Equation 15), the number of particles per second for each cloud along the span needs to be changed to ensure that the LWC is constant from root to tip. This is an artefact of the MRF conditions wherein the freestream velocity is imposed as a function of radius. Figure 9 depicts a simplified schematic of the injection clouds.

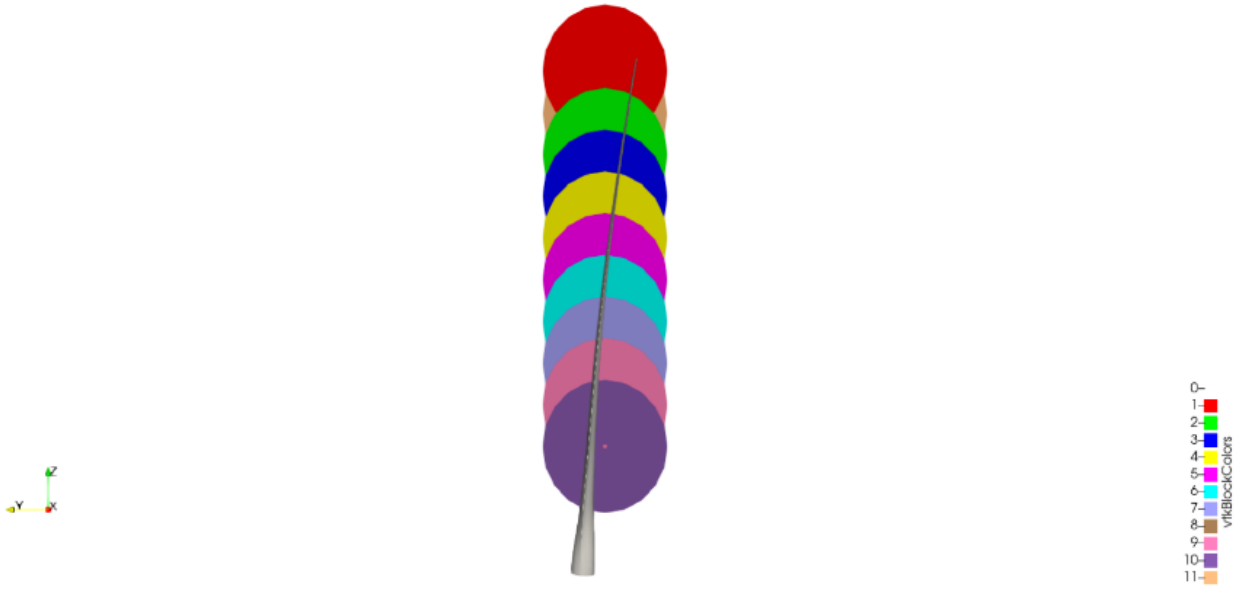

Figure 9. Clouds used for particle injection for MRF cases

Each cloud has the different height, because of this difference in the height, the relative velocity of the blade is changing with the relation to the rotation velocity of the blade. We provide just a sample of this work in Table 6 below:

Table 6. Sample of the LWC for MRF case

Height	Relative velocity (m/s)	Rotating velocity (rad/s)	Area of each disk	particles in each cloud	Volumetric flow rate	LWC
120	67.2	0.56	28.28	69471.36	0.000261	0.137496
117	65.52	0.56	28.28	67734.57	0.000255	0.137496
114	63.84	0.56	28.28	65997.79	0.000248	0.137496
111	62.16	0.56	28.28	64261	0.000242	0.137496

5.2.1 Results of the IEA 15MW MRF simulations for two rain intensities and a cone angle of 4 degrees (cases 3D15MRF5C4 and 3D15MRF20C4)

For the conditions mentioned in the Table 7, two different rain intensity conditions are studied. The first condition employs a rain intensity of 5 mm/h, which is considered as a normal rain condition.

Table 7. Initial conditions and rain characteristics

Rain conditions	Wind speed (m/s)	Omega (rad/s)	Rain intensity (mm/h)	LWC (g/m^3)	Simulated time (s)
Normal rain	11.4 m/s	0.56	5	0.34374	3,600
Heavy rain	11.4 m/s	0.56	20	1.10144	3,600

The particle diameter distribution that hit the blade are shown in Figure 10, where different colours represent different spanwise portions of the blade. The particle diameters that hit the blade deviate slightly from the injected particle diameter distribution (dashed line). The higher impact force observed towards the blade tip (shown in Figure 12) may be attributed to higher relative velocities as well as the

larger amount of total hits, which is confirmed by Figure 11 where the number of impacts per unit area at different positions along the blade are illustrated. The particle diameters are distinguished by different colours Figure 12 also shows that there are more particle impacts on the suction side of the blade. The highest impact is again seen around the local leading edge of the blade (indicated by the dotted lines).

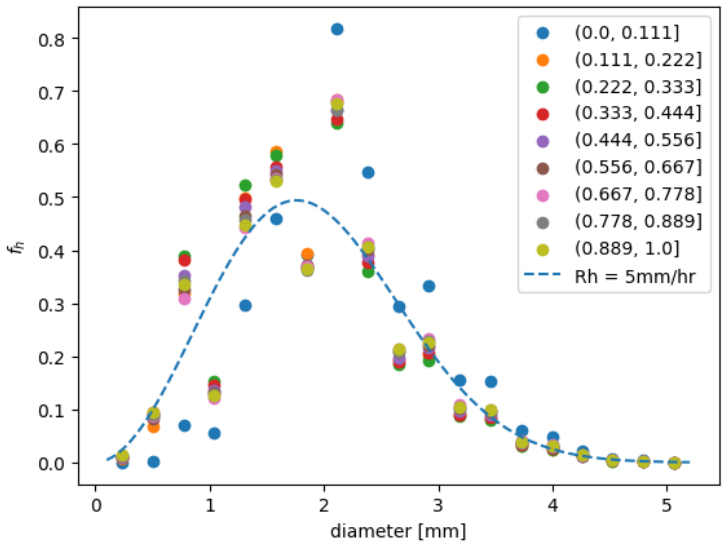

Figure 10. Particle diameter distribution that hit the blade for Rh=5mm/h (case 3D15MRF5C4)

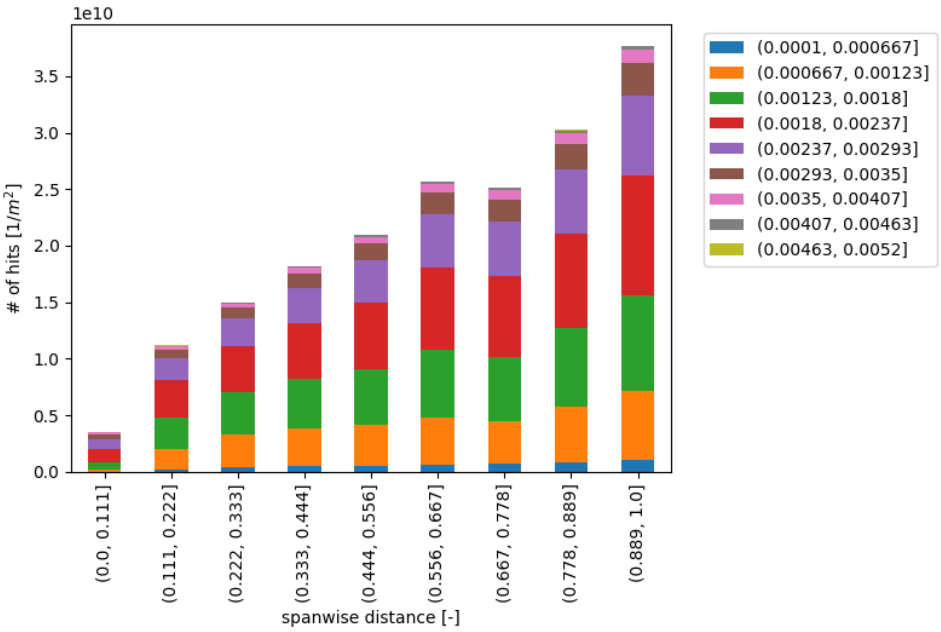

Figure 11. Number of hits per unit area for different section on the blade for Rh=5mm/h (case 3D15MRF5C4)

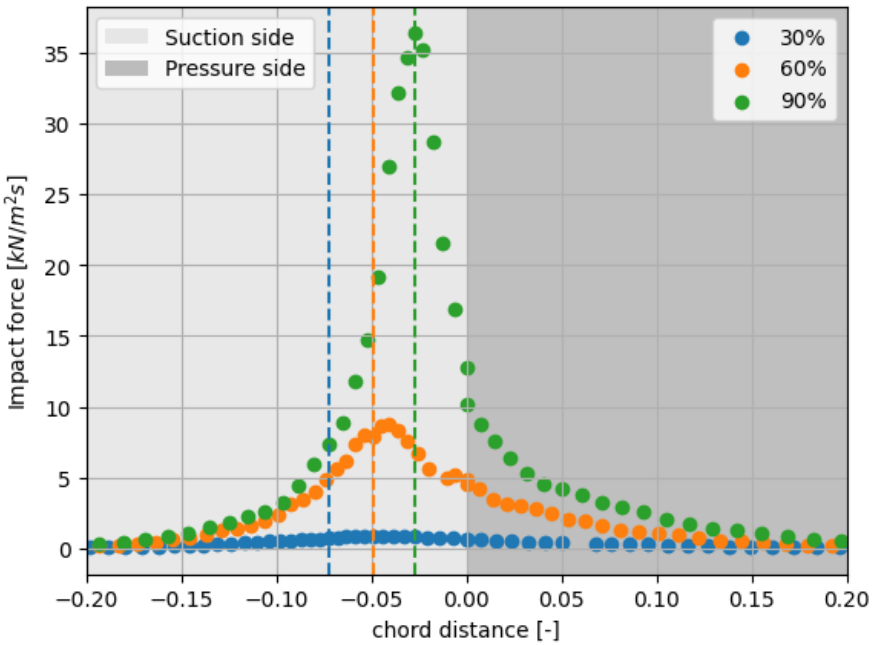

Figure 12. Impact force of the particles for three sections of the blade for Rh=5mm/h (case 3D15MRF5C4)

In a second case study, a rain intensity rate of 20mm/h is chosen, which is considered as heavy rain. Table 7 shows a higher number of impacts per unit area compared to the 5mm/h rain intensity case. Additionally, Figure 14 clearly indicates that the particle diameter has increased relative to the 5mm/h case (Figure 10).

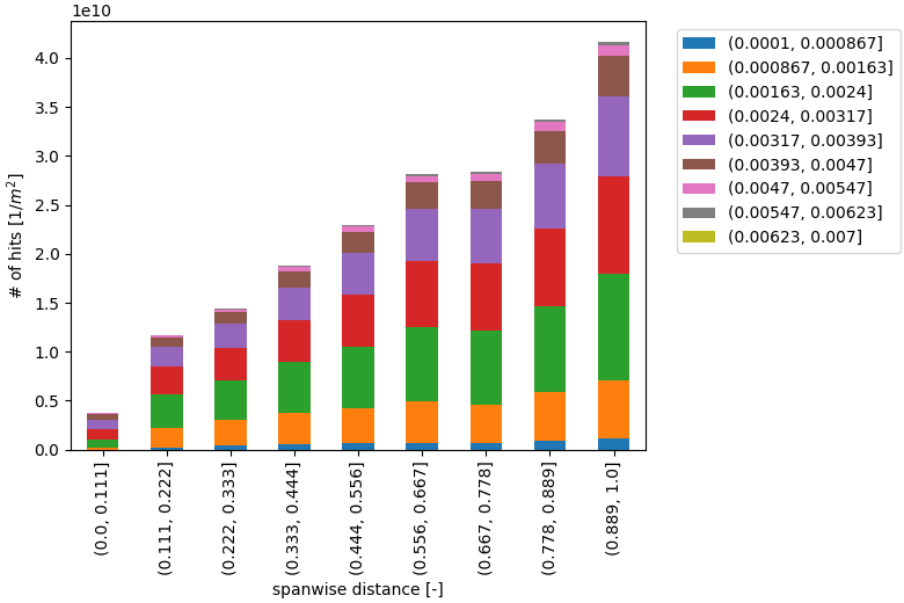

Figure 13. Number of hits per unit area for different section if blade for R_h=20mm/h (case 3D15MRF20C4).

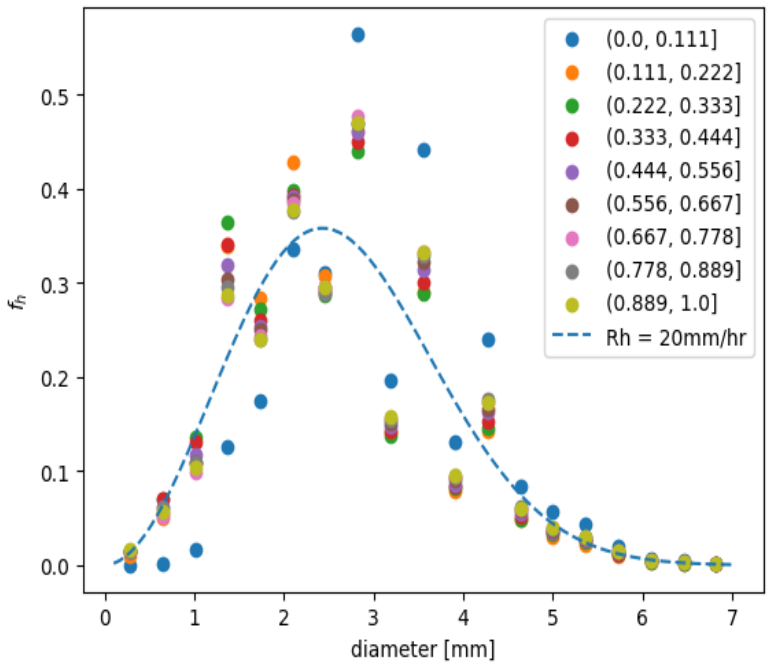

Figure 14. Particle diameter distribution that hit the blade for Rh=20mm/h (case 3D15MRF20C4).

As expected from the initial results, the heavy rain condition also shows a higher impact force near the tip and an increased impact concentration on the suction side, as observed in Figure 15.

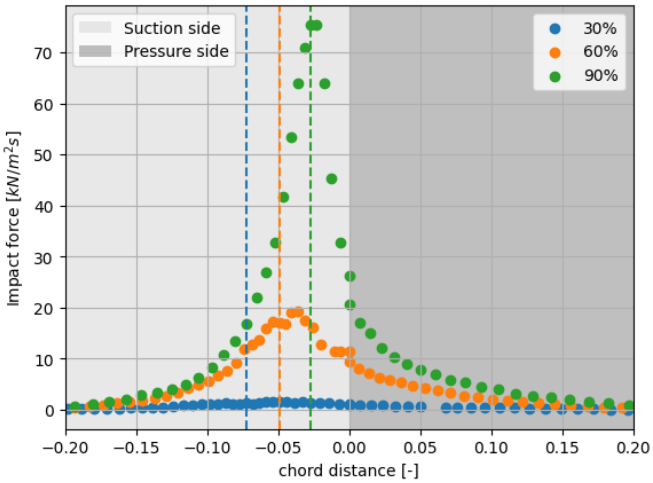

Figure 15. Impact force for three sections of blade for R_h=20mm/h (case 3D15MRF20C4).

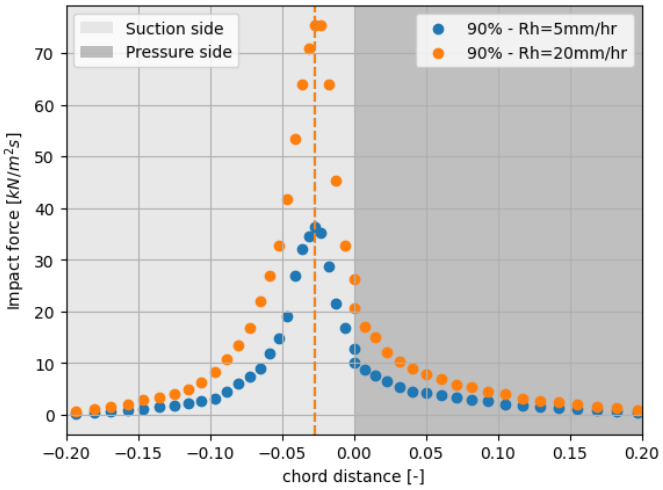

Figure 16. Impact force for Rh=5mm/h and R_h=20mm/h (case 3D15MRF20C4)

Normal and heavy rain conditions are compared in Figure 16 for a blade section of 90% span. It can be observed that (as expected) the rain intensity rate increases the impact force.

5.2.2 Results of the IEA 15MW MRF simulations for two rain intensities and a cone angle of 0 degrees (cases 3D15MRF5C0 and 3D15MRF20C0)

Table 8. Initial conditions for the IEA 15MW MRF case with a cone angle=0°

Omega	0.8 rad/s
Inlet velocity	10 m/s
Blade length	117 m
Solid wall	No slip
Cone angle	0 degrees
Left and right	120° periodic rotation
Simulation run time	3600 s

In this case different initial conditions are used, which corresponds to a slightly below rated operating condition. The corresponding settings are summarized in Table 8. For this case also two different rain conditions are used. Firstly, the rain **intensity** rate of 5mm/h is shown. Figure 17, Figure 18 and Figure 19 present the same plots as those under the previous conditions.

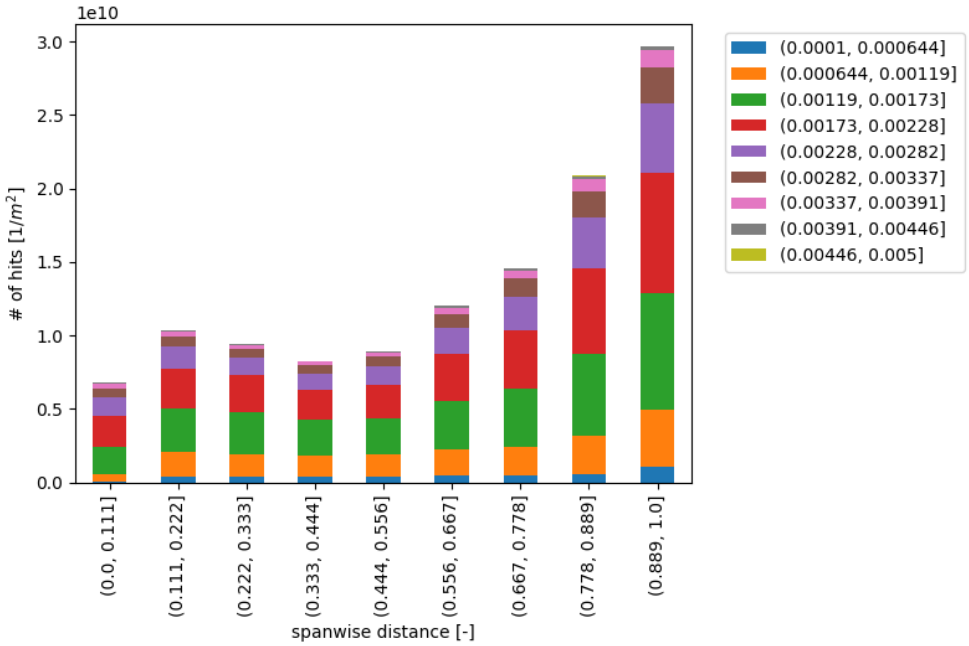

Figure 17. Number of hits per unit area for different sections of the blade for Rh=5mm/h (case 3D15MRF5C0)

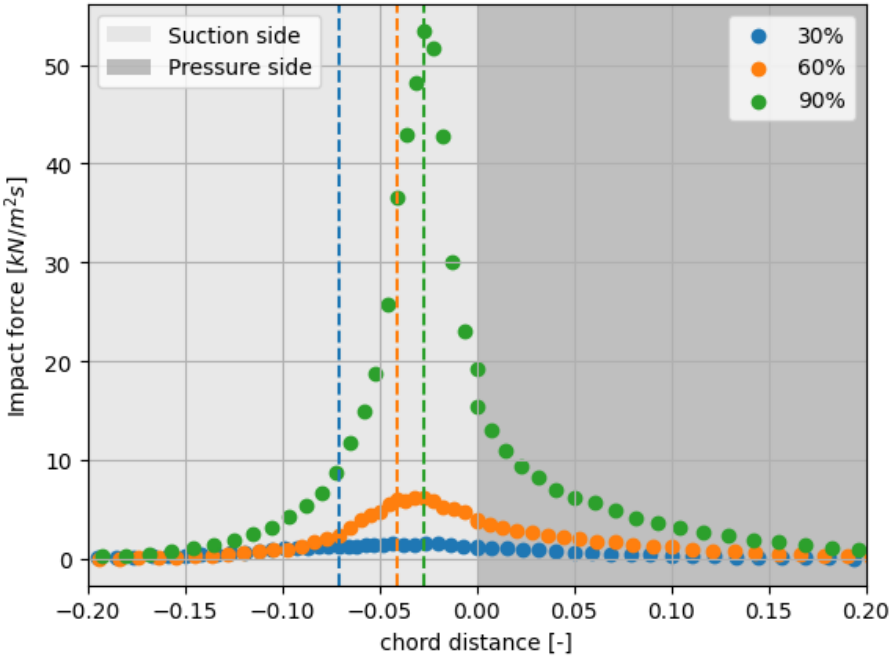

Figure 18. Impact force of the particles for three sections of blade for R_h=5mm/h (case 3D15MRF5C0).

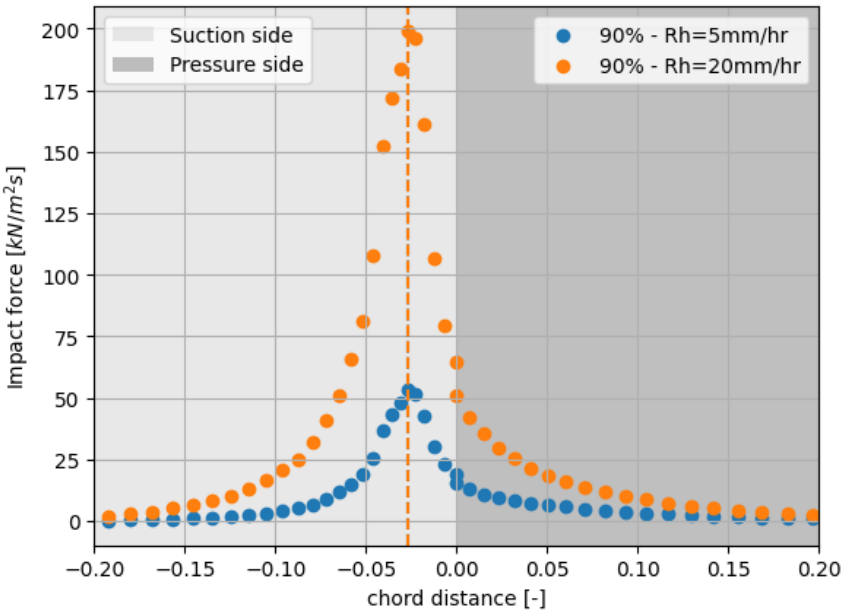

Figure 19. Impact force for two different conditions for R_h=5mm/h and 20mm/h (cases 3D15MRF5C0 and 3D15MRF20C0).

Similar results are shown for a rain intensity rate of 20mm/h (cf. Figure 20 to Figure 22).

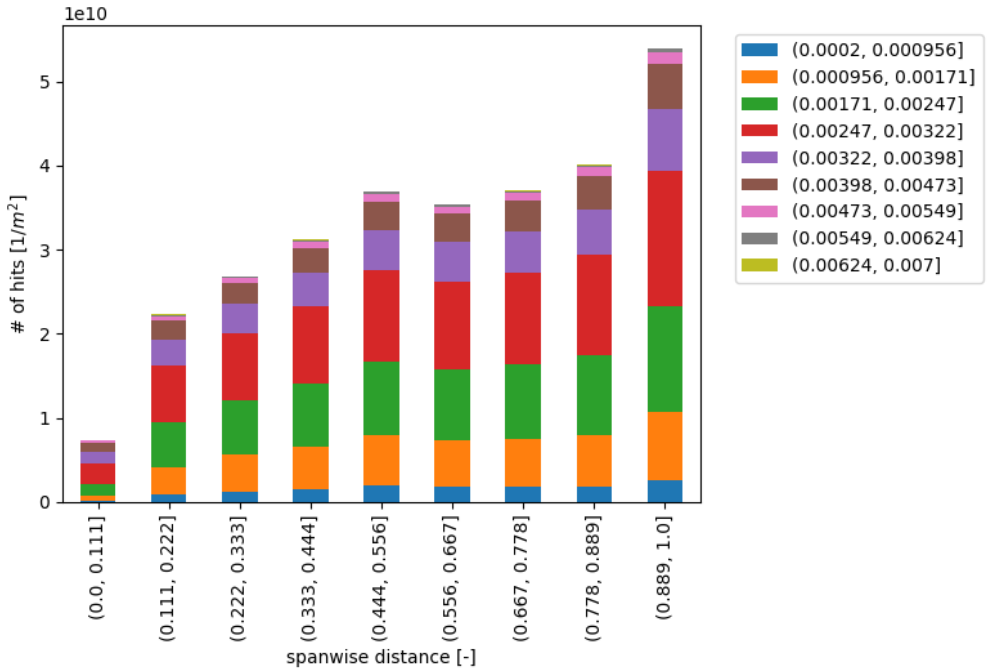

Figure 20. Number of hits per unit area for different section of the blade for R_h=20mm/h (3D15MRF20C0)

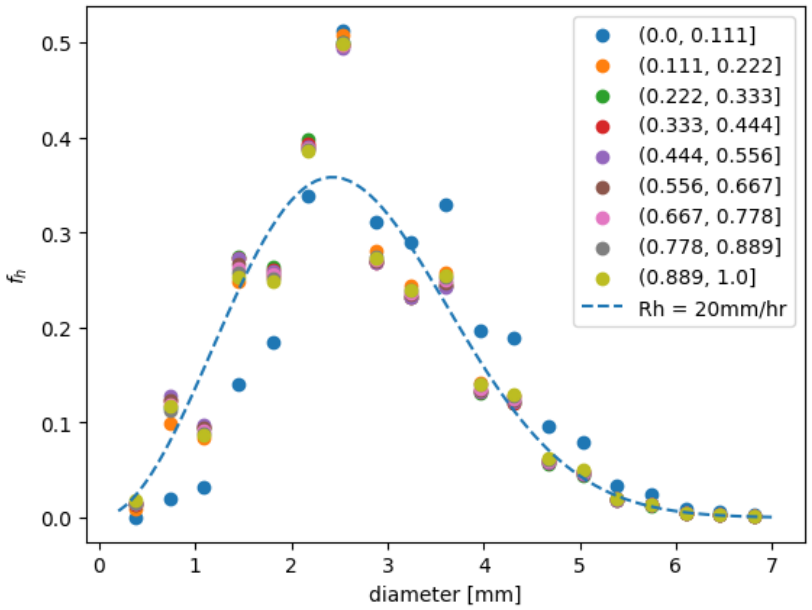

Figure 21. Particle diameter distribution that hit the blade for R_h=20mm/h (case 3D15MRF20C0).

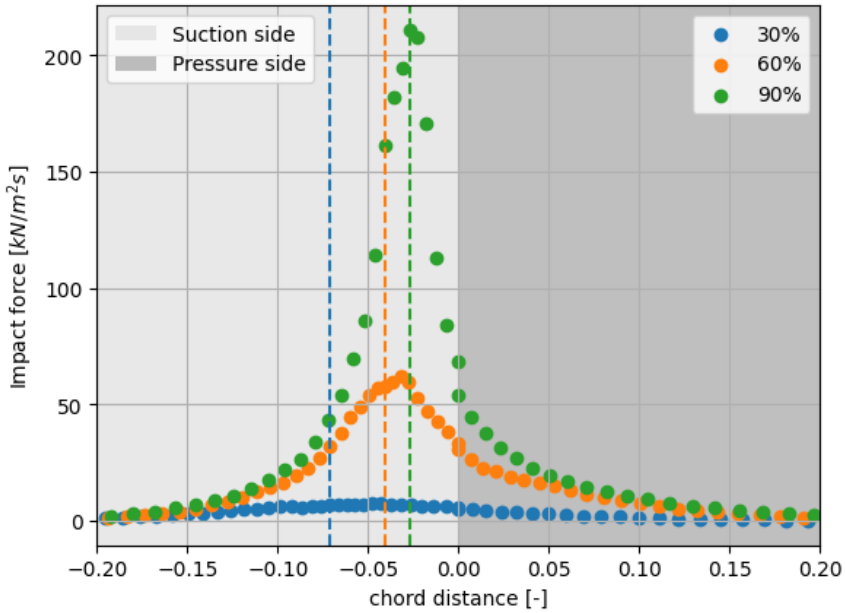

Figure 22. Impact force of the particles for three sections of blade for R_h=20mm/h (case 3D15MRF20C0).

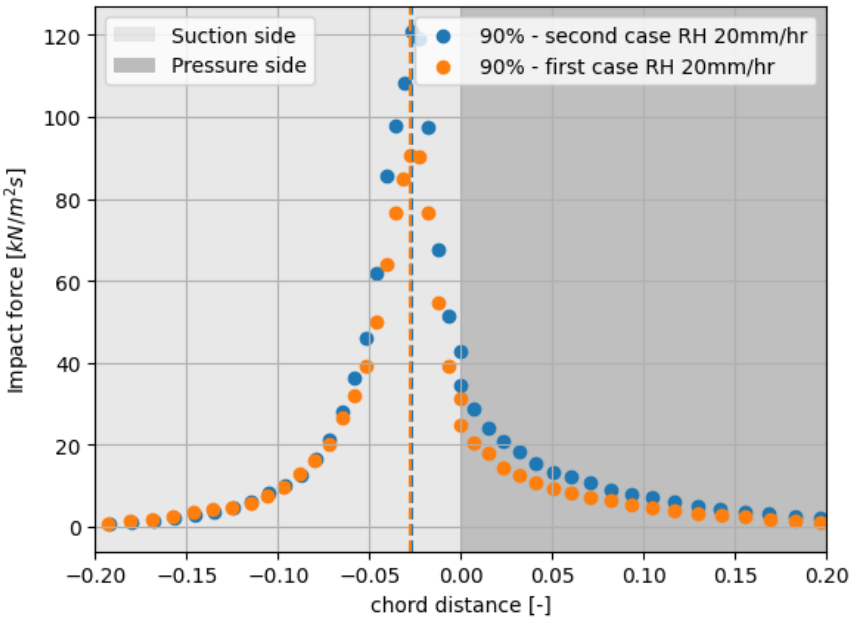

Figure 23. Impact force for two cone angles and omegas at R_h=20mm/h (case 3D15MRF20C4 in orange and 3D15MRF20C0 in blue).

According to the conditions of the second case, which has a higher omega related to the first case, we were expecting to have more impact force and more hits in the second case. Figure 23 and Figure 24 show that the amount of impact force for the crucial section of the blade, in the second case the maximal value is almost doubled compared to the first one.

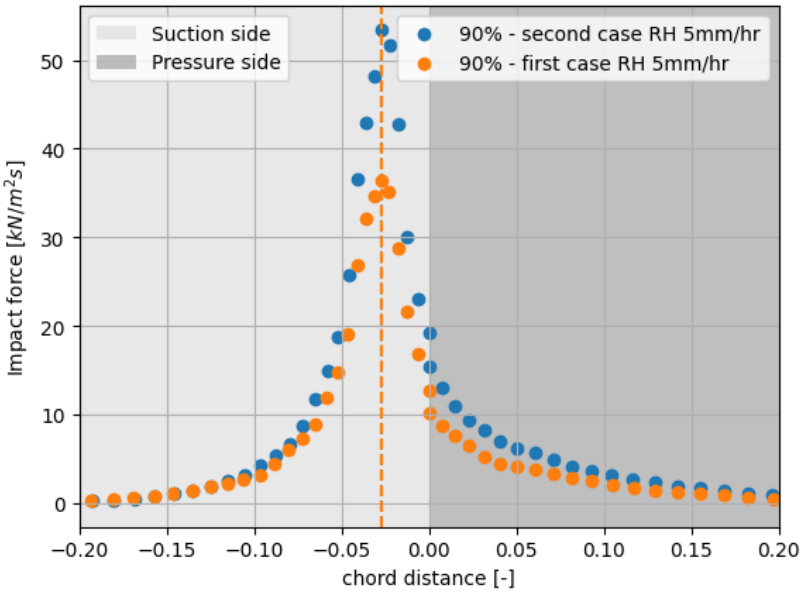

Figure 24. Impact force for two cone angles and omegas at R_h=5mm/h (case 3D15MRF5C4 in orange and 3D15MRF5C0 in blue

The cumulative particle hit locations for 5mm/h and 20mm/h are plotted side by side in Figure 25. This shows the impact of heavy rain on the particle distributions; specifically, the fact that heavy rain has a wider band of impact respective to the leading edge, and also that the number of hits increase with increasing rain intensity.

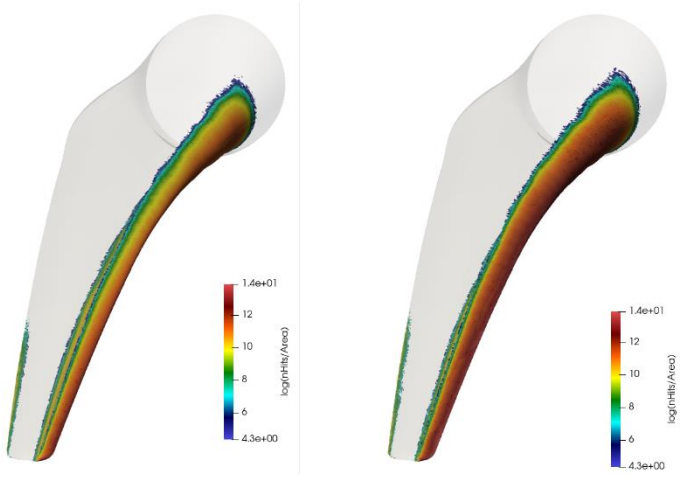

Figure 25. Impact locations on the blade (left: R_h=5mm/h and right: R_h=20mm/h) for the IEA 15MW turbine with a 0° cone angle using the MRF approach

To compare the different rain conditions and the two operating conditions, where the first case involves slower rotation and a cone angle of 4 degrees, we observe the following:

1. **Rain Conditions:** Higher rain intensity increases the number of impacts and the total force acting on the blade.
2. **Operating Conditions:** A higher rotational speed results in greater impact forces and a higher number of impacts. This is expected since, in the second case, the blade rotates faster, leading to higher impact velocities, which in turn increases the impact forces.

5.2.3 Cross-comparison of 2D and 3D MRF simulations of the IEA 15MW blade

Figure 26 and Figure 28 correspond to the MRF case, slower case with the cone angle for the section that shares the same conditions and shape as the 2D airfoil case (cf. Figure 5 and Figure 7). The 2D plots have been copied here for ease of comparison (See Figure 27 and Figure 29 below).

For both 5mm/h and 20mm/h, the 2D and 3D peak impact forces are very similar. However, for both normal and heavy rain, the 3D (MRF) bladed simulations lead to a much wider distribution of forces; i.e. further away from the leading edge. We postulate that the three-dimensional nature of flow on a blade, i.e. spanwise flow, is the major cause of this difference. One may also conclude from this that 2D simulations will underestimate the chordwise extent of raindrop impacts and hence also underestimate the spatial extent of erosion damage.

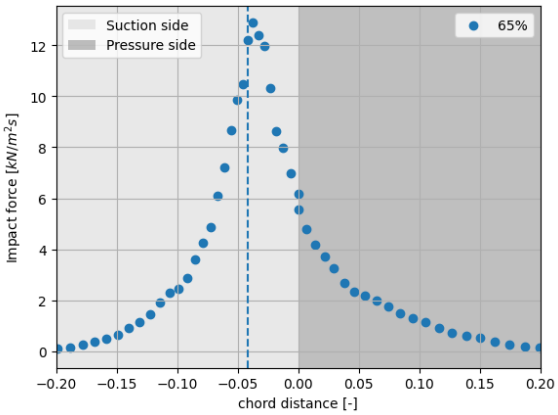

Figure 26. MRF R_h=5mm/h (case 3D15MRF5C4)

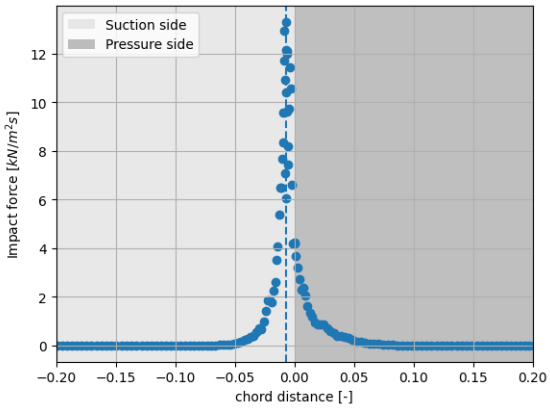

Figure 27. Impact force of the particles for the 2D airfoil for R_h=5mm/h (case 2D15A5). Copy of Figure 5.

For the lower rain intensity rate of 5mm/h, a similar maximal impact force is present. This does not hold true for the higher rain intensity rate of 20mm/h, which has its highest peak at 26kN/m^{2}s for 3D MRF and 35kN/m^{2}s for the 2D case. For higher rainfall rates, the 2D simulations hence not only underpredicts the spatial extent of potential damage, but also overpredicts the peak impact force, and hence will lead to faster erosion-onset estimations.

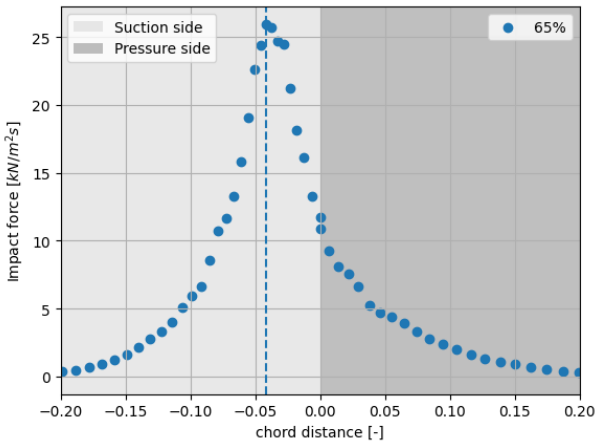

Figure 28. MRF Rh=20mm/h (case 3D15MRF20C4)

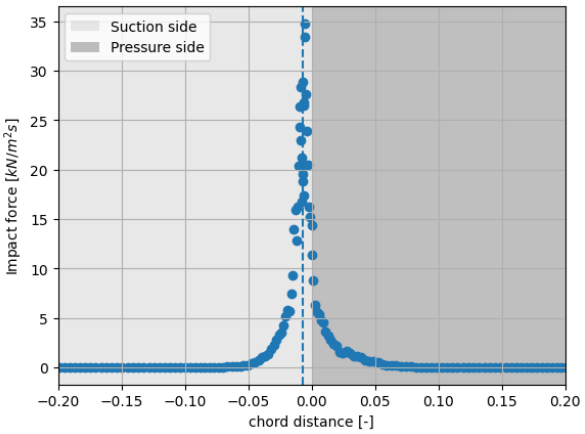

Figure 29. Impact force of the particles of the 2D airfoil for R_h=20mm/h (case 2D15A20). Copy of Figure 7

This comparison provides compelling evidence to support the use of MRF simulations rather than a series of 2D simulations for predicting spanwise erosion on wind turbine blades.

5.3 Full-turbine simulations

As in Section 0, the two wind turbines selected for this part of the work are the NREL 5MW and IEA 15MW wind turbines.

Both wind turbines are generated using in-house meshing software. The blade meshes were created using the bladeBlockMesher utility, which converts 2D sectional meshes into a 3D structure volume mesh, consisting of purely hexahedral cells. The toolbox windTurbineMesher uses the blade meshes to compose a full turbine setup using five different mesh regions that communicate using a sliding mesh interface. Those five regions are given by three blade meshes, a rotor mesh and a far-field mesh. All mesh regions, except the blade meshes, are hexa-dominant. The distribution of cells is given in Table 9. In both setups the domain measures 5 rotor diameters upstream and 15 rotor diameters downstream. The sides are located 3.5 rotor diameters from the rotational center.

Table 9. Mesh details of the NREL 5MW and IEA 15MW setups.

Turbine	NREL 5MW	IEA 15MW
Number of blade cells	3 x 3.56 million	3 x 10.43 million
Total cells	26.46 million	60.16 million

The incompressible, transient flow is simulated using the hybrid Spalart-Allmaras delayed detached eddy simulation method. To advance the solution in time, a second order implicit backward method is applied. Spatial discretization makes use of a second-order accurate Gauss linear scheme for the gradient terms and a first-order Gauss upwind scheme for the divergence terms.

In all the full-turbine cases there is just one big cloud of particles that approach the blades with the fixed LWC of 5mm/h.

5.3.1 NREL 5MW full rotor simulation (case 3D5FR5)

To approach the final goal of simulating a large 15MW turbine, this study first considers the computationally cheaper NREL 5MW turbine. The table below lists the initial conditions of this case.

Table 10. Initial conditions for case 3D5FR5.

Omega	1.27 rad/s
Inlet velocity	11.4 m/s
Blade length	61.5 m
Solid wall	No slip
Simulation run time	239 s
Case name	3D5FR5

The results for the normal rain condition with a rainfall intensity of 5 mm/h are presented in the following figures. As in the MRF case, we have divided our results into three different plots.

Figure 30 illustrates the number of impacts per unit area at various positions along the blade. It is evident that the trend observed in the full turbine simulation aligns with that of the MRF case.

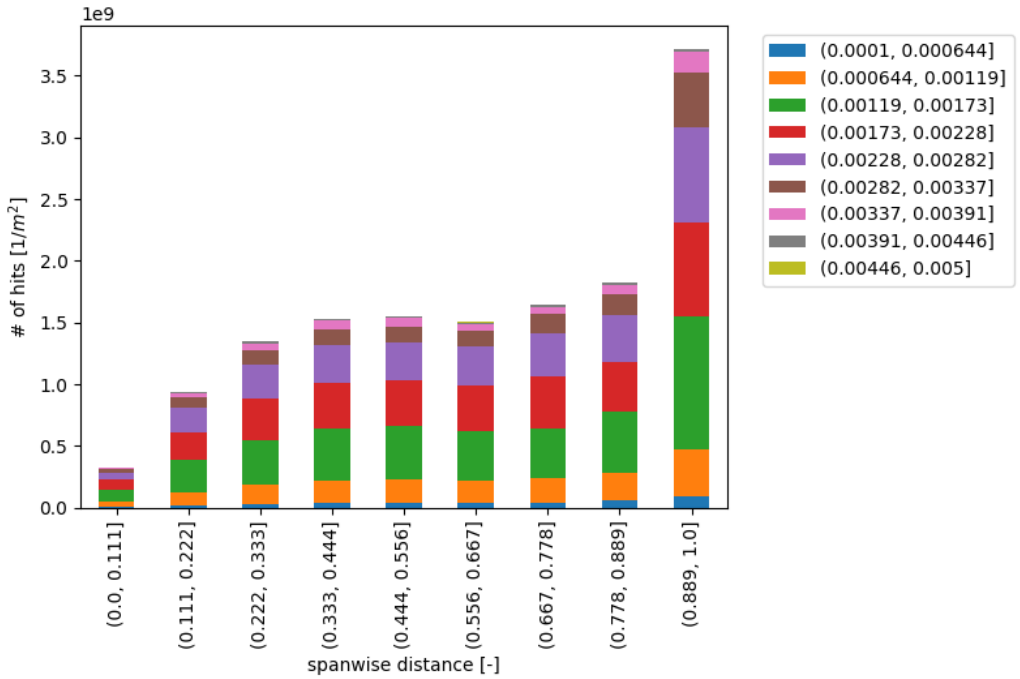

Figure 30 . Number of hits per unit area for different section of the blade for Rh=5mm/h (case 3D5FR5)

Figure 31 presents the impact force across three sections of the blade, showing an increase with spanwise distance. The data appears slightly noisier compared to the MRF case, which is expected due to the difference in total simulation runtime—3600s for the MRF case versus 239s in this case.

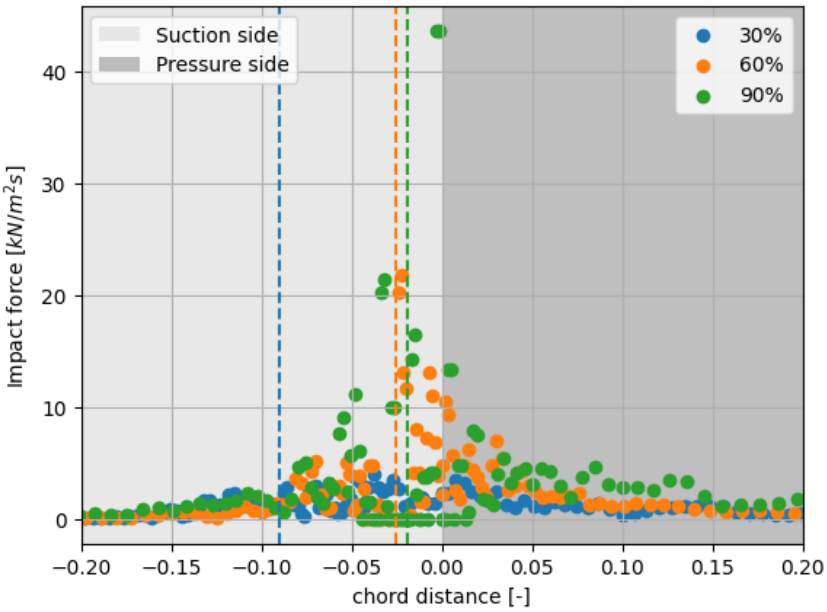

Figure 31. Impact force of the particles for three sections of blade for Rh=5mm/h (Case 3D5FR5).

In Figure 32, the particle diameters impacting the blade are shown, with different colours representing various spanwise portions of the blade. It is evident that the particle diameters that reach the blade slightly deviate from the injected particle diameter distribution, as indicated by the dashed line.

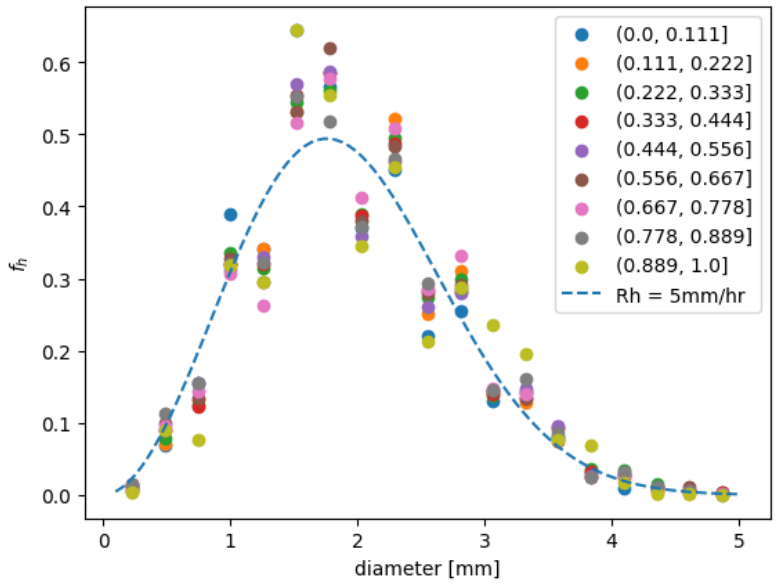

Figure 32. Particle diameter distribution that hit the blade for Rh=5mm/h (case 3D5FR5)

The studies also take into account the cumulative number of impacts for all three blades together. With this consideration, the results exhibit better scaling relative to simulation time, which is significantly more computationally expensive in the full turbine case.

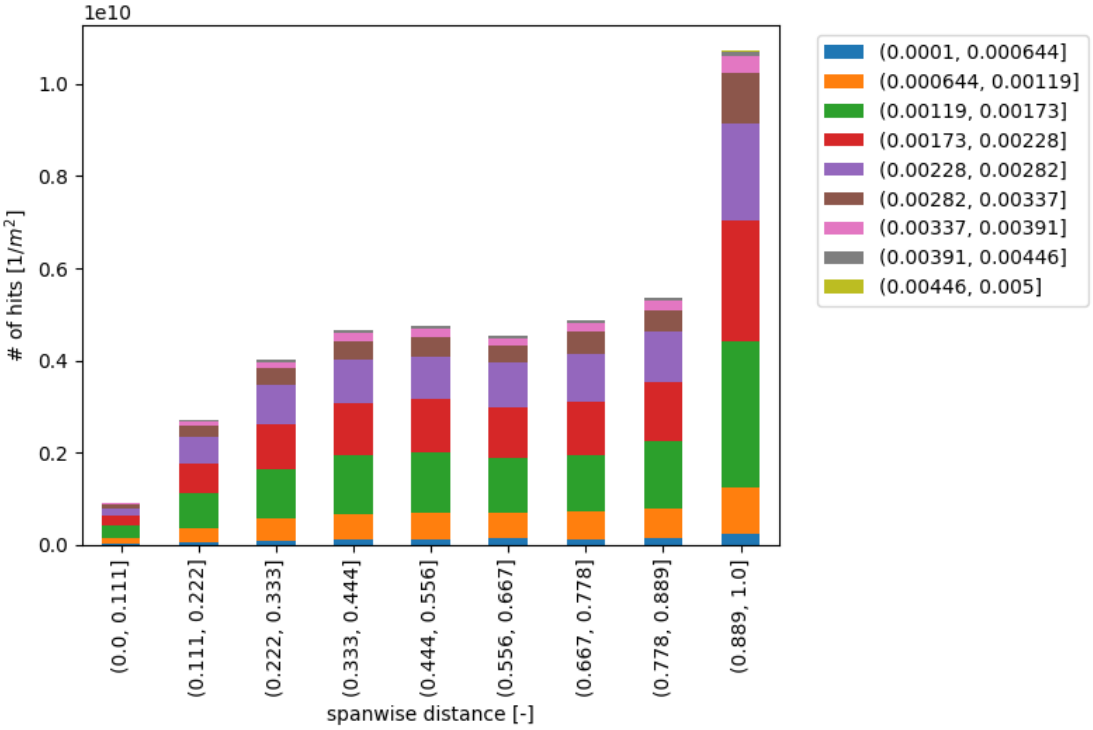

Figure 33. Average number of hits per unit area for all three blades with different section of the blade for Rh=5mm/h (case 3D5FR5).

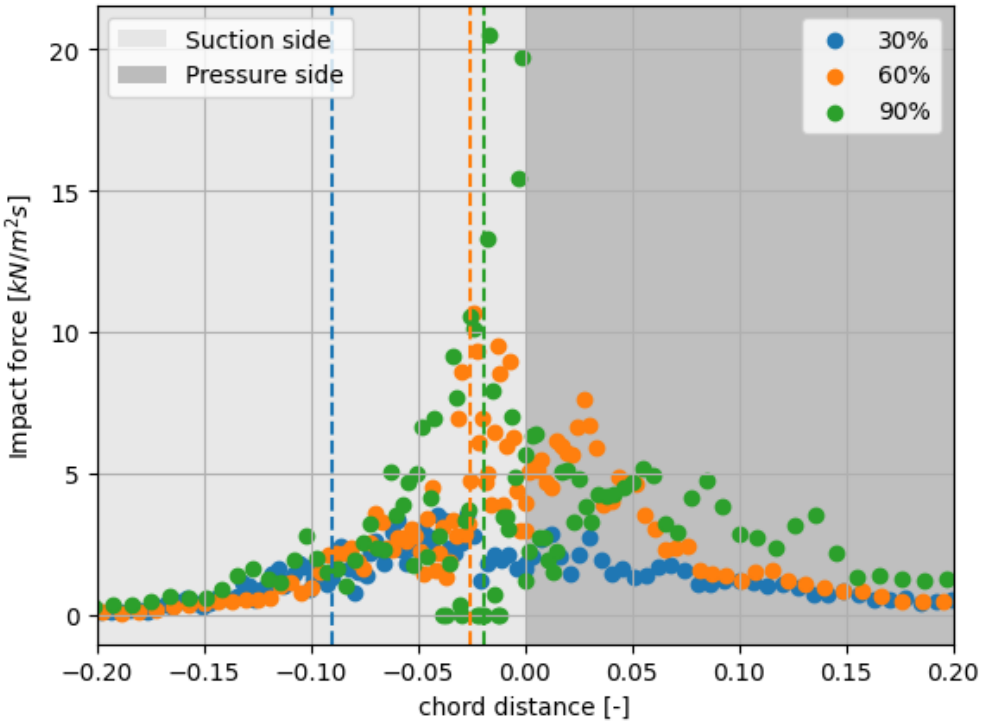

Figure 34. Average. Impact force of the particles for three blades and sections of blade for Rh=5mm/h (case 3D5FR5).

The total number of impacts, as shown in Figure 35, as well as in Figure 23 and Figure 13 for the MRF case, follows the same trend. This consistency confirms that the injection assumptions and methodologies used in both cases are reliable and coherent.

Additionally, in the impact force figures, such as Figure 36 for the three-blade case and Figure 25, we observe that the impact force is higher near the tip compared to sections closer to the root. Furthermore, like the MRF case, the suction side experiences greater impact forces.

5.3.2 IEA 15MW full rotor simulation (case 3D15FR5)

In the case of the IEA 15MW turbine, the injection method and liquid water content (LWC) are the same as in the NREL case. A single cloud of particles, consisting of different particle diameters and a fixed LWC, is introduced into the flow field, which is then transported toward the turbine by the velocity field of flow.

Table 11. Operating conditions for the 15MW IEA full rotor case

Omega	0.8 rad/s
Inlet velocity	10 m/s
Blade length	120 m
Solid wall	No slip
Simulation run time	114 s
Case name	3D15FR5

The results from the IEA 15MW case are still in the early stages and have not yet fully converged to match the results of the NREL and MRF cases. This case has only been run for half the simulation time of the NREL case. In Figure 37, we observe the early-stage impact distribution, averaged over the three blades.

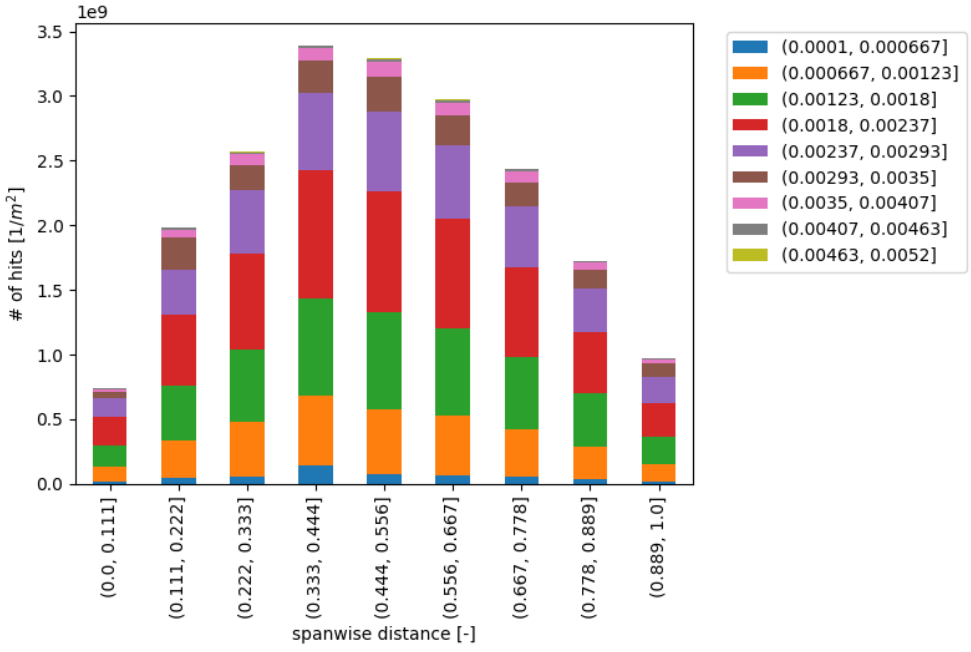

Figure 35. Average number of hits per unit area for all three blades with different section of the blade for R_h=5mm/h (case 3D15FR5).

According to Figure 38 the impact force remains higher near the tip, primarily due to the increased impact velocity in that region. If the total number of impacts is scaled and the simulation runs for more than 300 seconds, the results are expected to become smoother, resembling the ideal case observed in the MRF simulation.

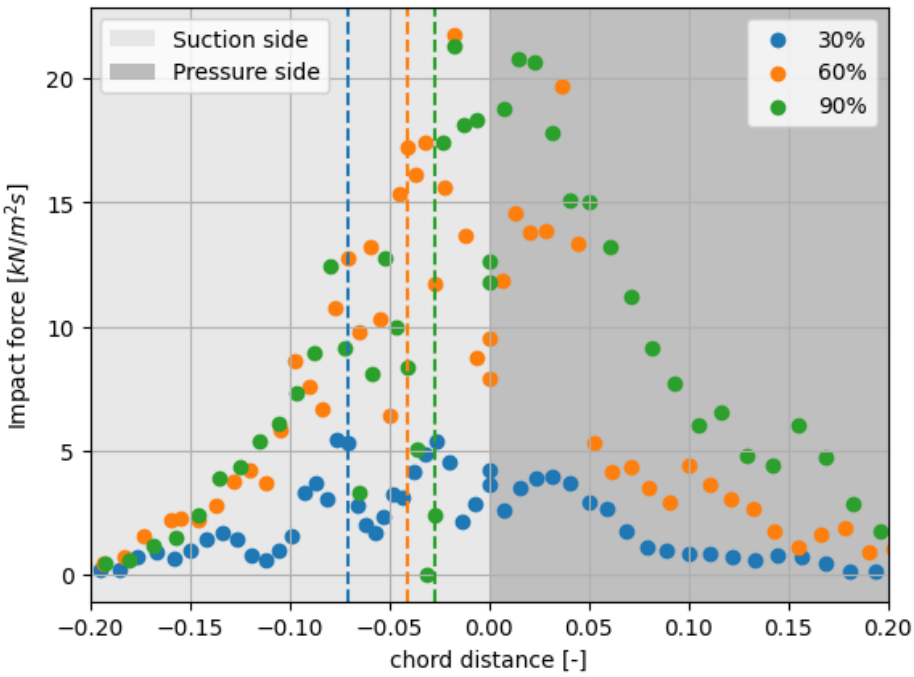

Figure 36. Average. Impact force of the particles for three blades and sections of blade for R_h=5mm/h (case 3D15FR5).

For the particle diameter distribution shown in Figure 39 the results are generally consistent with those from the other cases. However, in some sections, deviations from the theoretical input distribution are observed.

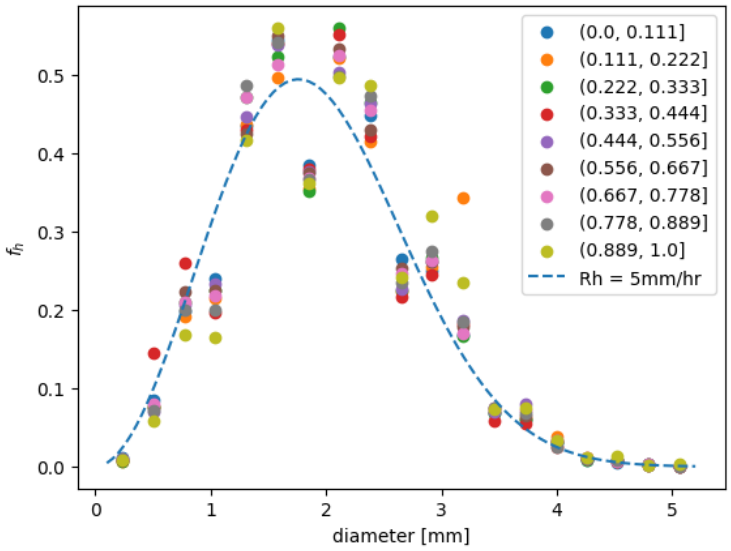

Figure 37. Particle diameter distribution that hit the blade for R_h=5mm/h (case 3D15FR5)

5.3.3 Comparing MRF (case 3D15MRF5C0) and full rotor simulation (case 3D15FR5) for the IEA 15MW turbine

The MRF and full-rotor simulations of the IEA 15MW turbine are compared in this section. The cumulative particle impacts have been extracted and plotted on the blade. A comparative view from the blade tip is shown in Figure 38. The colour map for both cases are defined as ln (n_i) where n_i is the

number of particle hits per unit area. The colour difference between the MRF and full rotor results arise from the fact that full rotor simulation ran for a shorter time.

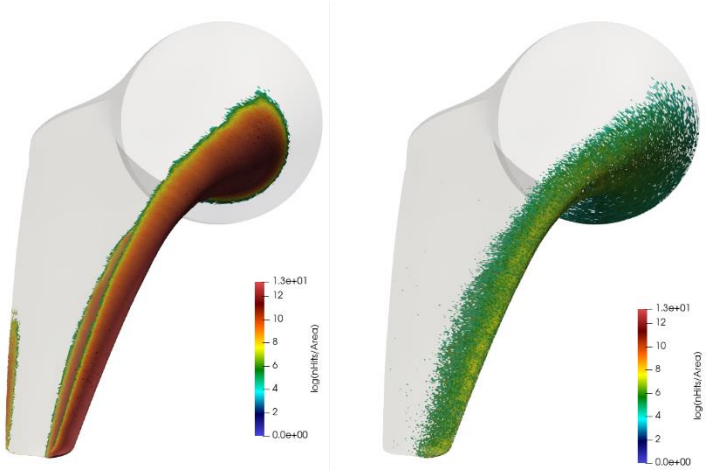

Figure 38. Map of particle impacts for MRF (left – case 3D15MRF5C0) and unsteady, full-turbine case (right – case 3D15FR5) for R_h=5mm/h

5.3.4 Comparing the IEA 15MW (case 3D15FR5) and NREL 5MW (case 3D5FR5) full-rotor simulation results

The full-rotor simulations of the NREL 5MW and IEA 15MW turbines are compared in this section. The cumulative particle impacts have been extracted and plotted on the respective blades. A comparative view from the blade tip is shown in Figure 39. Both cases have a very similar impact pattern around the leading edge, however the differences between them should be more apparent in the impact forces due to the differences in tip speed (around 80m/s for NREL and 100m/s for IEA turbine respectively).

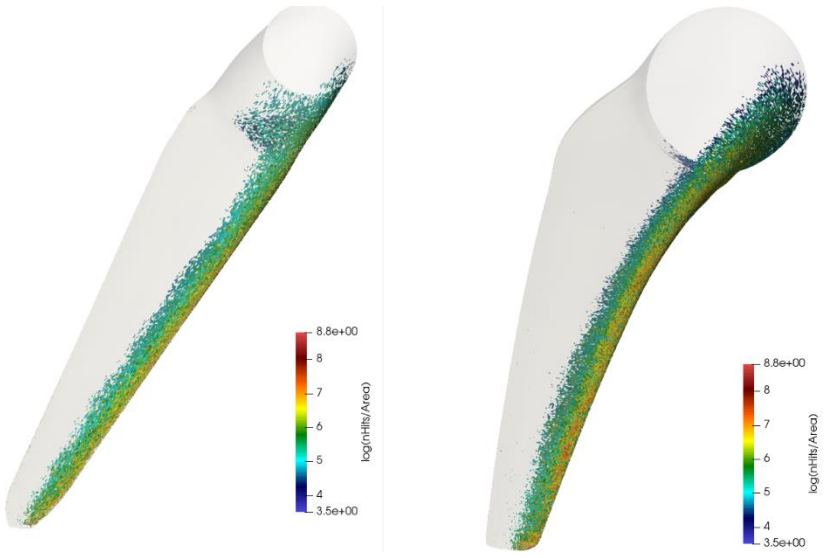

Figure 39. Map of particle impacts for NREL 5MW (left – case 3D5FR5) and IEA 15MW (right – case 3D15FR5) unsteady, full-turbine cases for R_h=5mm/h

6 Summary and conclusions

In this task, nine main cases have been studied covering three levels of simulations namely 2D airfoils, 3D steady single blade and 3D unsteady full rotor. Three rain intensity values are included with the corresponding rain distribution. Despite the technical challenges and the delays, the main objectives of the study have been achieved. In addition to typical similarity parameters such as Re (Reynolds number), the LWC is kept consistent across the cases with respect to the target rain intensity. Having such consistency allows at least for a loose comparison across cases.

The 2D simulations are the least demanding in terms of computational resources. Although they gave very good insights, they predict a narrow and sharp distribution of rain impact forces around the leading edge. On the other hand, both 3D steady single blade and 3D unsteady rotor cases show a wider spread of the impact force around the leading edge. This difference can be attributed to the spanwise flow which is not present in the 2D case. Comparing the single blade steady simulations and the full-rotor simulation showed a wider spread of the impact forces. This can be explained by the unsteady model used in the full-rotor case which captures some of the very large-scale turbulence structures.

As can be seen in many observations from actual turbines, the erosion is always concentrated around the leading edge which agrees with all the cases. However, only the full-rotor unsteady cases showed some significant impact of the pressure side. Both 2D and single blade cases predicted the impact mostly on the suction side. This deviation can also be due to the unsteady flow behaviour. Having said that, a much longer simulation is needed to confirm such a preliminary conclusion.

It is evident based on the single blade cases and the full-rotor that the local rain diameter distribution on the blade surface is highly correlated to the free-stream rain distribution. This supports the existing damage models which use such distributions and ignore the local effects spanwise.

One significant difference between the NREL 5MW case and the IEA 15MW is the spread of the impact force. It is much wider in the IEA 15MW case. Although, it can be eliminated that it is due to the shorter simulation run, it can also be the result of the difference of the leading-edge radius (The NREL blade consists of airfoils with a sharper leading edge). IWES is studying this effect further in WP6.1 as part of the airfoil design process.

7 Appendix

7.1 0.5mm/h MRF results

Results for a rain intensity rate of **0.5mm/h** using MRF (case 3D15MRF05C4):

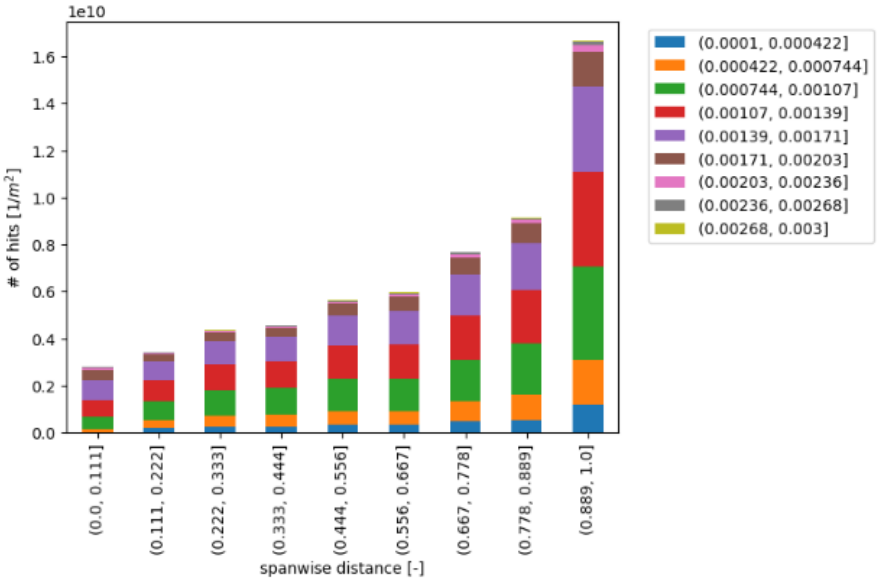

Figure 40 .Number of hits per unit area for different sections if blade for R_h=0.5mm/h.

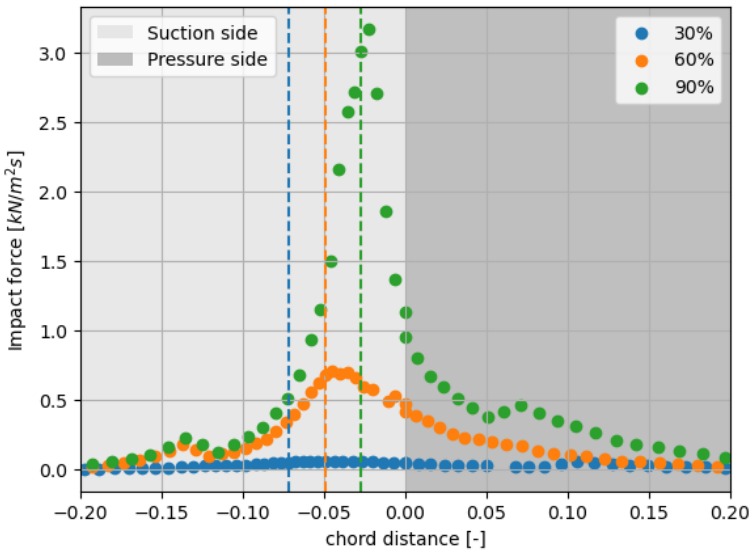

Figure 41. Impact force of the particles for three sections of blade for R_h=0.5mm/h, dashed lines represent the leading edge.

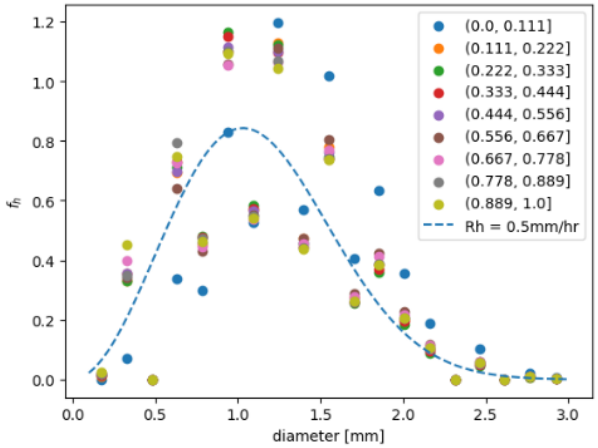

Figure 42. Particle diameter distribution that hit the blade for R_h=0.5mm/h.

8 References

1 Gimenez, Juan M. and Idelsohn, Sergio R. and Oñate, Eugenio, *Fast prediction of rain erosion in wind turbine blades using a data-based computational tool*, , J Hydrodyn, Vol. 36, No. 3, 2024, pp 504-.518, doi: 10.1007/s42241-024-0044-4

2 Clayton T. Crowe, *Multiphase flows with droplets and particles*, CRC Press, 2nd EDd., Boca Raton, ISBN 978-1-4398-4050-4 978-1-4398-4051-1

3 V. M.Boiko, A. A. Pivovarov, and S. V. Poplavski, *Measurement of gas velocity in a high-gradient flow, based on velocity of tracer particles*, Combust Explos Shock Waves, Vol. 49, No. 5, pp. 548-554, 2013, doi: 10.1134/S0010508213050067

4 R. Clift, and W.H. Gauvin, *Motion of entrained particles in gas streams*, Can J Chem Eng, Vol. 49, No. 4, 1971, doi: 10.1002/cjce.5450490403

5 Y. Cao, Z. Wu, and Z. Xu, *Effects of rainfall on aircraft aerodynamics*, Progress in Aerospace Sciences, Progress in Aerospace Scienceso, Vol. 71, , pp. 85-127, 2014, doi: 10.1016/j.paerosci.2014.07.003

6 J.S. Marshall and W. Mc.K Palmer, *The distribution of raindrops with size*, Journal of Meteorology, Vol. 5, No. 4, 1948, pp. 165-166, doi: 10.1175/1520-0469(1948)005<0165:TDORWS>2.0.CO;2

7 B.A. Campbell and G.M. Bezos, Steady-State and Transitional Aerodynamic Character-istics of a Wing in Simulated Heavy Rain, NASA Technical paper 2932, 1989

8 A.H. Markowitz, *Raindrop Size Distribution Expressions*, J. Appl. Meteor., Vol. 15, No. 9, 1976, pp. 1029-1031, doi: 10.1175/1520-0450(1976)015<1029:RSDE>2.0.CO;2

9 A. Castorrini, P. Venturini, and A. Bonfiglioli, *Generation of Surface Maps of Erosion Resistance for Wind Turbine Blades under Rain Flows*, Energies, Vol. 15, No. 15, 2022, pp. 5593, doi: 10.3390/en15155593

10 H. Law and V. Koutsos, Leading edge erosion of wind turbines: Effect of solid airborne particles and rain on operational wind farms, Wind Energgy, Vol. 23, No. 10, 2020, pp. 1955-1965, doi: 10.1002/we.2540

11 E. Gaertner, J. Rinker, L. Sethuraman, F, Zahle, B. Anderson, G.E. Barter, N.J. Abbas, F. Meng, P. Bortolotti, W, Skrzypinski, *IEA wind TCP task 37: definition of the IEA 15-megawatt offshore reference wind turbine*, 2020, National Renewable Energy Lab. (NREL), Golden, CO (United States)

12 J. Jonkman, S. Butterfield, W. Musial and G. Scott, *Definition of a 5MW Reference Wind Turbine for Offshore System Development*, NREL/TP--500--38060, 947422, 2009, doi: 10.2172/947422